Early Permian high-K calc-alkaline volcanic rocks from NW Inner Mongolia, North China: geochemistry, origin and tectonic implications

Xiaohui Zhang, Simon A. Wilde, Hongfu Zhang, et al.

Journal of the Geological Society 2011; v. 168; p. 525-543
doi: 10.1144/0016-76492010-094

Journal of the Geological Society, London, Vol. **168**, 2011, pp. 525–543. doi: 10.1144/0016-76492010-094.

Early Permian high-K calc-alkaline volcanic rocks from NW Inner Mongolia, North China: geochemistry, origin and tectonic implications

XIAOHUI ZHANG[1]*, SIMON A. WILDE[2], HONGFU ZHANG[1] & MINGGUO ZHAI[1]

[1]*State Key Laboratory of Lithospheric Evolution, Institute of Geology and Geophysics, Chinese Academy of Sciences, PO Box 9825, Beijing 100029, China*

[2]*Department of Applied Geology, Curtin University of Technology, Perth, WA 6845, Australia*

**Corresponding author (e-mail: zhangxh@mail.iggcas.ac.cn)*

Abstract: Knowledge of the characteristics of the extensive late Palaeozoic volcanic rocks across the northern China–Mongolia tract is essential for understanding the tectonic evolution and continental crustal growth in the Central Asian Orogenic Belt. This geochronological and geochemical study documents the Early Permian mafic and felsic volcanic rocks from northwestern Inner Mongolia. The mafic rocks form two magma series with distinctive geochemical characteristics; one showing large ion lithophile element (LILE) enrichment relative to high field strength elements (HFSE) and an asthenosphere-like Sr–Nd–Pb isotopic signature, and the other featuring an elevated Nb and lithospheric isotopic signature. This result indicates that two mantle source components are involved in the magma generation: the subduction-related metasomatized asthenosphere and lithospheric mantle. The felsic rocks show strong enrichment of LILE and light REE, depletion in HFSE, and indistinguishable isotopic compositions from mafic ones. Such features are consistent with partial melts of mixed sources composed of predominant juvenile basaltic underplates and minor ancient crustal materials. These mafic and felsic rocks constitute a post-subduction high-potassium calc-alkaline magmatic suite possibly under a geodynamic regime of Palaeo-Asian Ocean slab breakoff. This regime not only provides a feasible trigger for the flipping of subduction polarity in the Solonker suture zone, but also presents a favourable venue for vertical continental crustal growth.

The tectonic evolution of orogenic belts is typically marked by changes in the compositions of the associated magmatism (Harris *et al.* 1986; Bonin 2004; Wang *et al.* 2004). This is best exemplified by the temporal and spatial shift from subduction-related calc-alkaline to intraplate-type alkaline magmatism, as widely documented by post-collisional to post-orogenic igneous associations in most orogenic belts of various ages around the world (Sylvester 1989; Bonin *et al.* 1998; Coulon *et al.* 2002; Bonin 2004; Wang *et al.* 2004; Duggen *et al.* 2005; Clemens *et al.* 2009; Kuscu & Geneli 2010; Zhang *et al.* 2010*a*). Of this magmatic spectrum, the most instructive one may be high-K calc-alkaline to alkali-calcic mafic and felsic igneous suites that show indistinguishable mantle-like isotopic signatures. They commonly form a major constituent of late orogenic to post-collisional magmatism and indicate that the orogen is in the process of collapse (Altherr *et al.* 2000; Roberts *et al.* 2000; Ferré & Leake 2001; Bonin 2004; Chen & Arakawa 2005; Clemens *et al.* 2009; Topuz *et al.* 2010; Zhang *et al.* 2010*a*). Moreover, they generally represent a crustal continuum growth of magmatic underplating (Frost *et al.* 2001*a*; Chen & Arakawa 2005; Zhang *et al.* 2010*a*). Therefore, petrogenetic studies of such mafic and felsic magmatic suites in ancient orogenic belts can not only provide important constraints for understanding the tectonic evolution of these belts, but also document significant information in fully characterizing the growth and differentiation of the continental crust.

The Central Asian Orogenic Belt (Fig. 1a) has been regarded as a huge accretionary collage dominated by juvenile Palaeozoic granitoid rocks and characterized by a series of late Precambrian to early Mesozoic suture zones that developed between the Siberian and North China cratons (Sengör *et al.* 1993). As a major palaeo-plate boundary in Asia that stretches northeastwards over 2500 km in Mongolia and China (Li 2006), the Solonker suture zone has been widely regarded as the site of final closure of the Palaeo-Asian Ocean (Fig. 1b; Sengör *et al.* 1993; Xiao *et al.* 2003, 2009). Most recently, Jian *et al.* (2010) proposed its evolution as a Permian intraoceanic arc–trench system. However, many essential issues still remain uncertain, such as the tectonic evolution of the opposite-facing continental blocks, the subduction polarity and the mechanism for its switch.

In terms of continental growth, the Central Asian Orogenic Belt has been widely accepted as Earth's largest site of Phanerozoic juvenile continental crustal formation (e.g. Jahn 2004). Specifically, both lateral accretion of arc complexes in subduction zones and vertical addition by underplating at the crust–mantle interface are advocated as the main mechanisms of crustal growth in this region (Jahn 2004). However, their relative importance in evolved tectonic environments is the subject of continuing debate (Jahn 2004; Chen & Arakawa 2005; Windley *et al.* 2007; Zhang *et al.* 2008, 2010*a*).

In this paper, we present new geochronological, geochemical and isotopic data for the late Palaeozoic volcanic rocks from Sonidzuoqi in northwestern Inner Mongolia, which is tectonically located in the northern block of the northern China–Mongolian tract, to constrain their petrogenesis and to investigate the tectonic environment in which they developed, as a contribution to our understanding of the above controversial tectonic and crustal evolution issues.

Geological background

The Central Asian Orogenic Belt represents a giant accretionary orogen that extends from the Urals to the Pacific and from the

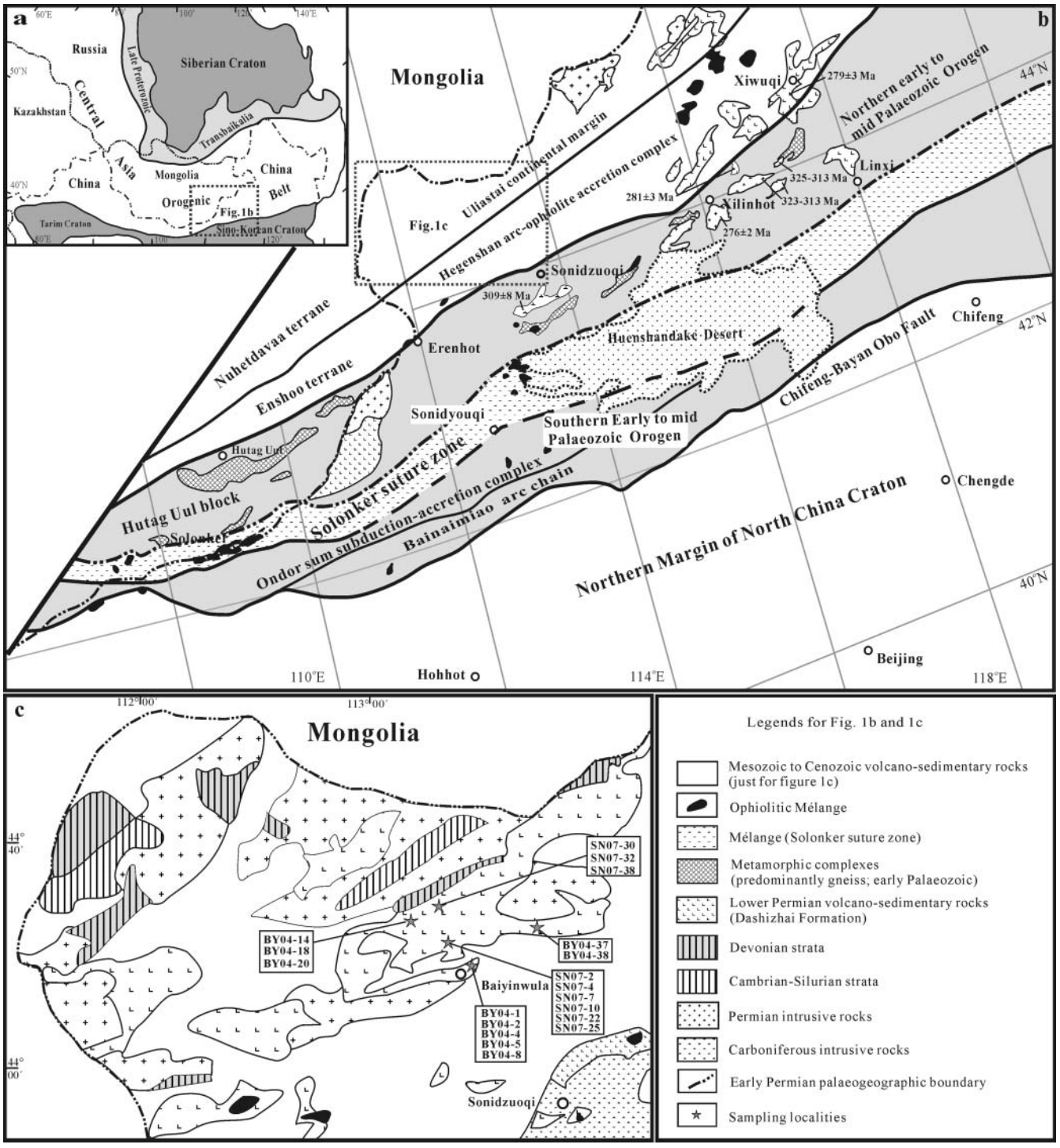

Fig. 1. (**a**) Tectonic framework of the north China–Mongolian segment of the Central Asian Orogenic Belt (modified after Jahn 2004). (**b**) Sketch geological map of the northern China–Mongolia tract (modified after Badarch *et al.* 2002; Miao *et al.* 2007; Xiao *et al.* 2009; Jian *et al.* 2010). Sources for the cited zircon ages for Carboniferous and Permian magmatic rocks are as follows: 325–313 Ma, Bao *et al.* (2007); 323–313 Ma, Liu *et al.* (2009); 309 ± 8 Ma, Chen *et al.* (2000); 281 ± 3 Ma and 279 ± 3 Ma, Zhang *et al.* (2008); 276 ± 2 Ma, Shi *et al.* (2004) (**c**) Sketch geological map of the Sonidzuoqi area (modified after IMBGMR 1980), with the sample locations shown.

Siberian and East European cratons to the North China (or Sino-Korean) and Tarim cratons (Sengör *et al.* 1993; Windley *et al.* 2007). It mainly consists of island arcs, ophiolites, oceanic islands, accretionary wedges, oceanic plateaux and microcontinents comparable with those of circum-Pacific Mesozoic–Cenozoic accretionary orogens (Xiao *et al.* 2003; Windley *et al.* 2007). Numerous recent studies have reconstructed the tectonic setting and evolution of several segments of this giant orogenic

belt by restoring the local subduction–accretion and collision zones (Badarch *et al.* 2002; Xiao *et al.* 2003, 2009; Helo *et al.* 2006; Miao *et al.* 2007; Jian *et al.* 2008, 2010; Blight *et al.* 2010*a*,*b*).

The northern China–Mongolia tract lies along the central-eastern segment of the Central Asian Orogenic Belt. Its most prominent tectonic feature is the Solonker suture zone, which marks the final closure of the Palaeo-Asian Ocean and separates two opposite-facing continental blocks (Fig. 1b; Jian *et al.* 2010). The northern block includes the Hutag Uul Block of southern Mongolia (Badarch *et al.* 2002), the Uliastai Block, Hegenshan ophiolite–arc accretion complex and the Northern Orogen (early to mid-Palaeozoic) in northern China (Jian *et al.* 2008). The southern block comprises the Southern Orogen (early to mid-Palaeozoic) and the northern margin of the North China Craton (Jian *et al.* 2010).

To the north of the Solonker suture, the basement geology of southern Mongolia is characterized by island-arc, back-arc–forearc basin and accretionary prism terranes that accreted around a postulated Precambrian cratonic block, the Hutag Uul Block (Badarch *et al.* 2002). These terranes record the tectonic evolution of the northern margin of the Palaeo-Asian Ocean during the Palaeozoic, generally interpreted to have been above a northward-dipping subduction zone (Windley *et al.* 2007). This results in multiple phases of arc magmatic activity from Silurian to Late Carboniferous (Lamb & Badarch 2001; Helo *et al.* 2006; Yarmolyuk *et al.* 2008; Blight *et al.* 2010*a*,*b*). They were subsequently intruded by great volume of latest Carboniferous to Early Permian peralkaline granites (Kovalenko *et al.* 2006; Yarmolyuk *et al.* 2008; Blight *et al.* 2010*a*). The Uliastai Block consists of a basement of Proterozoic gneiss, schist and quartzite and Cambrian limestone and siltstone (Xiao *et al.* 2003, 2009). The early to mid-Palaeozoic Northern Orogen of northern China is characterized by a metamorphic complex (Chen *et al.* 2009), a suprasubduction-zone-type ophiolitic sequence (Jian *et al.* 2008; Zhang, X.H., *et al.* 2009) and an overlying Late Devonian conglomerate. The Hegenshan ophiolite–arc accretion complex contains variably foliated calc-alkaline plutons of Carboniferous age (Chen *et al.* 2000; Bao *et al.* 2007; Liu *et al.* 2009) and suprasubduction-zone-type ophiolitic rocks (*c.* 298–293 Ma) at Hegenshan (Miao *et al.* 2007, 2008). These units were then intruded by undeformed Early Permian alkaline rocks and A-type granites (Wu *et al.* 2002; Shi *et al.* 2004).

To the south of the Solonker suture, the early Palaeozoic Southern Orogen includes the Ondor Sum subduction–accretion complex with blueschist, a suprasubduction-zone-type ophiolite (*c.* 497–477 Ma) and the Bainaimiao arc chain (*c.* 488–438 Ma) (Jian *et al.* 2008). It is separated from the North China Craton by the Chifeng–Bayan Obo fault.

During late Palaeozoic times, the northern margin of the North China Craton experienced several magmatic events (Zhang & Zhai 2010, and references therein), such as Middle Devonian mafic and alkaline intrusions (Zhang *et al.* 2009*a*; Zhang *et al.* 2010*b*), Carboniferous foliated calc-alkaline plutons (Zhang *et al.* 2009*b*), Early Permian high-K calc-alkaline I-, S- and A-type intrusive rocks (Zhang & Zhai 2010, and references therein), and latest Permian to Early Triassic high-K calc-alkaline to alkaline intrusive rocks (Zhang *et al.* 2009*a*; Zhang *et al.* 2010*a*).

The Lower Permian volcanic–sedimentary sequences constitute a prominent geological feature in northern China (Fig. 1c), among which the volcanic rocks occur as dominant components and have been designated by a general name, the Dashizhai Formation (Shao *et al.* 2007). These successions mainly consist of lavas, tuffs and volcaniclastic rocks with a thickness varying from about 200 m to 1200 m. They also show lateral variations in lithology over the elongated region of Inner Mongolia. At Xilinhot and Xiwuqi in central Inner Mongolia (Fig. 1b), the volcanic rocks show a bimodal composition with dominant rhyolite–dacite and local basalt–andesite, with an extrusive age of *c.* 280 Ma (Zhang *et al.* 2008). At Linxi, the succession is dominantly composed of basalt, basaltic andesite, basaltic trachy-andesite and related tuffs and pyroclastic deposits (Zhu *et al.* 2001; Lü *et al.* 2002). In eastern Inner Mongolia, the Dashizhai Formation consists of predominant rhyolite and andesite and minor basic lavas (Shao *et al.* 2007). Overlying Upper Permian sedimentary formations spread across the suture zone and commonly include sandstone, siltstone and slate (Cope *et al.* 2005; Shen *et al.* 2006).

Field relations and petrography

Northwest Inner Mongolia is a critical area in the northern block (Fig. 1b) and its magmatic and tectonic evolution has a significant bearing on the correlation of the southern Mongolia continental margin to the west and the Uliastai continental margin to the east.

The Baiyinwula region is located *c*. 50 km NW of Sonidzuoqi town (Fig. 1c), which is at the margin of the Northern Orogen. Field relations show that Permian strata there overlie Devonian sedimentary rocks, and are intruded by a number of Mesozoic granitic intrusions and overlain by Cenozoic flood basalts (IMBGMR 1980). The strata have been divided by various investigators into two distinct formations (IMBGMR 1980; Jiang *et al.* 1995): the lower Baolige Formation, comprising a volcano-sedimentary association, and the upper Zhesi Formation, made up largely of sedimentary successions. The Baolige Formation is essentially equivalent to the Dashizhai Formation in northern China, and can be subdivided into three units, designated as A, B and C. Unit A, at the base of the formation, is about 200 m thick and is mainly composed of black to grey metaconglomerates, shales and siltstones with plant fragments. Unit B uncomformably overlies Unit A and has a thickness of more than 3000 m. It contains a lower section of basaltic to andesitic lavas and intercalated pyroclastic rocks, and an upper section of mainly dacitic to rhyolitic lavas and intercalated welded tuff sequences. Unit C is about 2000 m thick and consists of breccia-bearing tuff, tuffaceous sandstone and siltstone, with minor limestone and andesite interbeds. Overlying the Baolige Formation with angular unconformity is the Zhesi Formation, which is about 400 m thick and consists of light red limestone, white to yellow siltstone and fine- to medium-grained sandstone, with conglomerate-bearing coarse-grained sandstone and shale interbeds (bearing Early Permian (Asselian and Sakmarian) fossils).

Owing to low relief and poor field exposure, it is very difficult to establish the eruptive episodes in the volcanic sequences. We collected a few fresh rock samples for petrological and geochemical analyses from Unit B of the Baolige Formation at several scattered outcrops along a number of dry river-valleys, as detailed in Figure 1c. Consistent with previous qualitative description in the literature (IMBGMR 1980; Jiang *et al.* 1995), our petrographic observations and geochemical data reveal a bimodal composition distribution for the investigated volcanic rocks, with mafic and felsic suites. At the locality where samples SN07-2 to SN07-25 were collected, the sequence mainly consists of basalts and basaltic trachy-andesite in the lower part, and rhyolite in the upper part.

The mafic suite includes basalt, basaltic andesite and minor andesite, whereas the felsic suite mainly consists of rhyolite,

ignimbrite and crystal-bearing tuffs. The basalts and basaltic andesites are dark grey and commonly show a porphyritic texture with phenocrysts of olivine and pyroxene. Pyroxene phenocrysts are dominantly augite with a composition $Wo_{40-44}En_{39-43}Fs_{13-20}$. The groundmass is fine-grained to microcrystalline, consisting of plagioclase, pyroxene, amphibole and magnetite. Two andesite samples are grey–green, and display a porphyritic texture with 15–20 modal % phenocrysts of plagioclase, augite and hornblende in a hyalopilitic matrix of plagioclase, biotite and hornblende. Apatite, zircon and magnetite are common accessory minerals, whereas chlorite, epidote and calcite are typical alteration products.

The rhyolites and rhyodacites are brown to pink, and exhibit subaphyric to porphyritic texture with predominant feldspar phenocrysts up to 2–5 mm in diameter. The microgranular to felsophyric groundmass is mainly composed of aphanitic plagioclase, K-feldspar, quartz and some biotite. Accessory minerals include zircon, apatite, magnetite and ilmenite. Typical alteration minerals include late-formed sericite, albite and clay minerals.

Analytical methods

Major element compositions of minerals were measured on a JEOL JXA-8100 electron microprobe at the Institute of Geology and Geophysics, Chinese Academy of Sciences (IGGCAS). The operating conditions were: 15 kV accelerating voltage, 10 nA beam current and 3 μm spot diameter. Well-defined natural mineral standards were used for calibration.

Zircons were separated from a basaltic andesite (BY04-20) and a rhyolite (BY04-1) sample using standard density and magnetic separation techniques and purified by handpicking under a binocular microscope. Cathodoluminescence (CL) images were obtained for zircons prior to analyses, using a JXA-8100 microprobe at IGGCAS, to reveal their internal structures.

Zircon U–Pb dating was conducted by sensitive high-resolution ion microprobe (SHRIMP) using the SHRIMP II ion microprobe at Curtin University of Technology under standard operating conditions (six-scan cycle, 2 nA primary O_2^- beam, mass resolution *c*. 5000), following analytical procedures as described by Williams (1998). Data were processed using the SQUID (1.02) and ISOPLOT (Ludwig 2001) programs. Corrections of Pb/U ratios were made by normalization to zircon standard CZ3 ($^{206}Pb/^{238}Pb = 0.0914$, corresponding to an age of 564 Ma). The data were corrected for common lead using the measured ^{204}Pb. Uncertainties on single analyses are reported at 1σ level, whereas pooled ages are quoted at the 95% (2σ) level.

For geochemical and isotopic analyses, samples were ground in an agate mill to *c*. 200 mesh. Major oxides were analysed by X-ray fluorescence spectrometry (XRF) with a Phillips PW 2400 system at the IGGCAS. Trace element abundances were obtained by inductively coupled plasma mass spectrometry (ICP-MS) using a VG-PQII system also at the IGGCAS. Samples were dissolved in distilled HF + HNO_3 in 15 ml high-pressure Teflon bombs at 120 °C for 6 days, dried and then diluted to 50 ml for analysis. A blank solution was prepared and the total procedural blank was <50 ng for all trace elements. Indium was used as an internal standard to correct for matrix effects and instrument drift. Precision for all trace elements is estimated to be 5% and accuracy is better than 5% for most elements by analyses of the GSR-3 standard.

Sr and Nd isotopic compositions were measured by thermal ionization mass spectrometry (TIMS) using a Finnigan Mat 262 system at the IGGCAS, following the procedure described by Zhang *et al.* (2008). Procedural blanks were <100 pg for Sm and Nd and <500 pg for Rb and Sr. $^{143}Nd/^{144}Nd$ was corrected for mass fractionation by normalization to $^{146}Nd/^{144}Nd = 0.7219$, and $^{87}Sr/^{86}Sr$ ratios were normalized to $^{86}Sr/^{88}Sr = 0.1194$. The measured values for the BCR-2 Nd standard and NBS-987 Sr standard were $^{143}Nd/^{144}Nd = 0.512613 \pm 0.000012$ (2σ, $n = 3$) and $^{87}Sr/^{86}Sr = 0.710251 \pm 0.000011$ (2σ, $n = 5$) during the period of data acquisition.

For Pb isotope determination, the powders were dissolved in Teflon vials with purified HF at 120 °C for 6 days and then separated using anion-exchange columns (AG1X8, 200–400 resin) with diluted HBr as eluant. Repetitive analyses of NBS981 yielded $^{206}Pb/^{204}Pb = 16.917 \pm 0.008$, $^{207}Pb/^{204}Pb = 15.460 \pm 0.010$, $^{208}Pb/^{204}Pb = 36.617 \pm 0.011$. The Pb data were corrected based on the NBS981 recommended data. Precision of lead isotope ratios is within ±1‰.

Analytical results

Zircon U–Pb data

The results of SHRIMP zircon U–Pb analyses are listed in Table 1. Zircons from basaltic andesite sample BY04-20 range in size from 50 to 120 μm and are mostly sub-euhedral columnar crystals. In CL images, they typically show low, homogeneous luminescence with faint oscillatory zoning (Fig. 2a). Six analyses were conducted on six grains from this sample and gave low f_{206} values up to 0.75%. Measured U and Th are in the range 75–738 and 49–823 ppm, respectively, with the exception of analysis 2 (1587 and 2319 ppm). All six analyses have Th/U ratios between 0.66 and 1.46 and form a coherent group with a weighted mean $^{206}Pb/^{238}U$ age of 289 ± 3 Ma (MSWD = 0.21) (Fig. 2a).

Zircons from rhyolite sample BY04-1 are mostly clear, euhedral to subhedral, stubby to elongate prisms. They range in size from 80 to 150 μm and have length to width ratios between 1;1 and 3;1. They commonly exhibit strong magmatic oscillatory zoning (Fig. 2b). Twelve analyses were conducted on 12 grains from this sample and show low f_{206} values up to 1.04%. U and Th concentrations are in the range 107–914 and 60–947 ppm, respectively. All analyses give Th/U ratios between 0.58 and 1.46 and yield a weighted mean $^{206}Pb/^{238}U$ age of 287 ± 3 Ma with an MSWD of 0.35 (Fig. 2b).

Major and trace elements

Major and trace element analyses are presented in Table 2. As shown on the K_2O + Na_2O v. SiO_2 diagram (Le Maitre 1989) (Fig. 3a), these volcanic rocks display a bimodal geochemical distribution. Among 19 analysed samples, the mafic suite plots in the fields of basalt, basaltic andesite and andesite, whereas the felsic suite exclusively lies within the field of rhyolite.

The rocks from the mafic suite range from 49.4 to 58.9% SiO_2, with aluminium saturation index [ASI = molar Al_2O_3/($CaO + K_2O + Na_2O$)] of 0.73–1.06 and Mg-number of 32.0-52.4. Most samples belong to the high-K alkaline series on the K_2O v. SiO_2 plot (Fig. 3b). They also show a magnesian character (Fig. 3c) and range from calcic to alkali fields on the alkali–lime index (MALI = $Na_2O + K_2O - CaO$ by weight) plot (Fig. 3d) according to the classification of Frost *et al.* (2001*b*). In terms of trace elements, the basalts and basaltic andesites exhibit uniform chondrite-normalized REE patterns enriched in light REE (LREE) with La_N/Yb_N of 4–9.8 and small negative Eu anomalies (Eu/Eu* = 0.79–0.97; Table 2; Fig. 4a). In the primitive mantle-normalized trace element diagram (Fig. 4b), two basalt samples have patterns enriched in both large ion

Table 1. *SHRIMP zircon U–Pb data for the mafic (BY04-20) and felsic (BY04-5) samples from the Sonidquozi volcanic rocks*

Spot number	U (ppm)	Th (ppm)	Th/U	Pb (ppm)	f_{206} (%)	Isotopic ratios						Age (Ma)
						$^{207}Pb/^{206}Pb$	1σ	$^{206}Pb/^{238}U$	1σ	$^{207}Pb/^{235}U$	1σ	$^{206}Pb/^{238}U \pm 1\sigma$
BY04-20 basaltic andesite												
1	99	94	0.94	6	0.16	0.0536	0.0021	0.0471	0.0008	0.348	0.013	297 ± 4
2	1587	2319	1.46	113	0.75	0.0505	0.0009	0.0469	0.0007	0.326	0.007	295 ± 4
3	221	223	1.00	14	0.14	0.0513	0.0015	0.0462	0.0006	0.327	0.008	291 ± 4
4	706	808	1.14	45	0.17	0.0521	0.0007	0.0448	0.0004	0.321	0.006	282 ± 4
5	738	823	1.11	46	0.07	0.0542	0.0010	0.0446	0.0007	0.333	0.009	281 ± 5
6	75	49	0.66	4	0.01	0.0516	0.0022	0.0459	0.0007	0.327	0.015	290 ± 4
BY04-1 rhyolite												
1	107	60	0.58	4.2	1.04	0.0476	0.0035	0.0450	0.0008	0.300	0.021	284 ± 5
2	298	251	0.87	11.6	0.09	0.0542	0.0009	0.0455	0.0007	0.340	0.008	287 ± 4
3	201	145	0.74	7.7	0.36	0.0504	0.0015	0.0447	0.0007	0.310	0.009	282 ± 5
4	300	255	0.88	12.0	0.21	0.0506	0.0010	0.0464	0.0006	0.320	0.006	292 ± 5
5	341	329	1.00	13.4	0.45	0.0501	0.0011	0.0456	0.0007	0.310	0.008	287 ± 4
6	459	411	0.92	17.9	0.22	0.0521	0.0011	0.0453	0.0005	0.330	0.008	286 ± 5
7	914	945	1.07	36.0	0.21	0.0517	0.0009	0.0458	0.0008	0.330	0.008	289 ± 5
8	325	232	0.74	12.9	0.35	0.0515	0.0011	0.0459	0.0007	0.330	0.009	290 ± 4
9	377	284	0.78	14.7	0.02	0.0524	0.0008	0.0455	0.0005	0.330	0.006	287 ± 4
10	239	166	0.72	9.4	0.38	0.0497	0.0011	0.0457	0.0009	0.310	0.009	288 ± 5
11	669	947	1.46	25.8	0.14	0.0511	0.0006	0.0449	0.0008	0.320	0.007	283 ± 5
12	516	464	0.93	20.3	0.43	0.0522	0.0012	0.0457	0.0007	0.330	0.007	288 ± 5

f_{206}, percentage of common ^{206}Pb in the total measured ^{206}Pb.

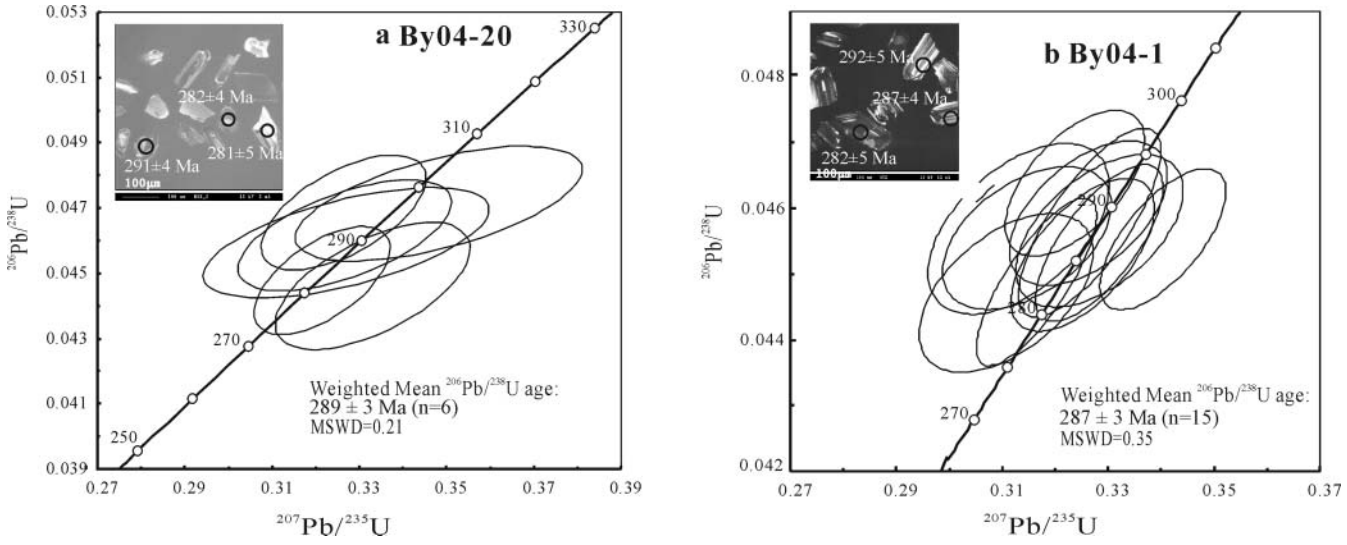

Fig. 2. Cathodoluminescence (CL) images of representative grains of analysed zircon and U–Pb zircon concordia diagrams for mafic sample BY04-20 (**a**) and felsic sample BY04-1 (**b**) from the Sonidzuoqi volcanic rocks.

lithophile elements (LILE; i.e. Rb, Ba, Sr, Th, U) and high field strength elements (HFSE; i.e. Nb, Ta), similar to those of ocean island basalts (OIB). The other basalt and basaltic andesite samples display patterns enriched in LILE but depleted in HFSE (Nb, Ta, Zr, Hf and Ti). Two andesite samples are characterized by high contents of Al_2O_3 and Na_2O, moderate MgO and Fe_2O_3*, and low contents of TiO_2 and P_2O_5, with moderate LREE enrichment ($La_N/Yb_N = 8.7–9.4$) and slight negative Eu anomalies ($Eu/Eu^* = 0.90–0.91$) (Fig. 4a). In the primitive mantle-normalized diagrams (Fig. 4b), they show significant enrichments in LILE (e.g. Rb, Ba, Sr, Th, U, LREE) and conspicuous depletion in Nb, Ta, and Ti.

The rhyolites have rather restricted ranges of SiO_2 (70.3–72.5%) and Al_2O_3 (13.8–15.4%), high alkalis ($K_2O + Na_2O = 8.51–9.99\%$), and low MgO (0.18–0.93%) and CaO (0.24–1.04%). They exhibit a high-K calc-alkaline character (Fig. 3b), with A/CNK of 0.97–1.29 and A/NK of 1.0–1.36. They range from magnesian to ferroan (Fig. 3c) and mainly plot in the alkali-calcic and alkali fields on the alkali–lime index plot (Fig. 3d). As for trace elements, they display chondrite-normalized REE patterns with moderate enrichments of LREE ($La_N/Yb_N = 5.5–9.1$) and slight negative Eu anomalies ($Eu/Eu^* = 0.68–0.91$) (Fig. 4c). In the primitive mantle-normalized diagram (Fig. 4d), they show enrichments in LILE (Rb, Ba, Th, U and LREE), depletion in Nb, Ta, P and Ti, and various concentrations of Sr.

Table 2. *Major and trace element data for the Sonidzuoqi volcanic rocks*

Sample:	BY04-2	BY04-14	BY04-18	BY04-20	SN07-2	SN07-4	SN07-10	SN07-30	SN07-32
Rock type:	B.A	B	B	B.A	B	B	B.A	A	A
SiO_2	54.78	50.04	49.39	56.91	51.53	51.86	56.27	58.46	58.91
TiO_2	2.01	2.33	2.43	1.06	1.86	1.78	1.07	0.90	0.90
Al_2O_3	16.88	15.99	15.66	17.73	16.14	15.76	17.71	16.28	16.25
$Fe_2O_3^T$	9.92	10.95	11.39	6.70	9.12	9.47	6.88	6.15	6.08
MnO	0.12	0.15	0.16	0.10	0.15	0.14	0.11	0.05	0.05
MgO	2.36	5.59	5.82	3.22	5.06	5.24	3.54	3.08	2.92
CaO	4.18	6.90	7.02	6.42	8.25	8.12	6.19	4.14	4.01
Na_2O	4.95	4.11	4.02	3.63	3.01	3.75	3.59	3.25	3.37
K_2O	2.55	1.83	1.88	1.57	1.65	1.82	1.85	2.60	2.32
P_2O5	0.53	0.71	0.73	0.41	0.58	0.49	0.40	0.27	0.26
LOI	2.13	1.02	1.05	1.72	2.18	1.54	1.92	4.38	4.47
Total	100.42	99.62	99.55	99.47	99.53	99.97	99.53	99.56	99.54
Mg-no.	32	50.3	50.3	48.8	52.3	52.4	50.5	49.8	48.8
ASI	0.91	0.75	0.73	0.92	0.74	0.69	0.92	1.04	1.06
Sc	20.4	20.8	23.3	17.5	29.7	27.9	17.0	14.7	14.8
V	135	166	181	151	220	202	152	163	162
Cr	2.16	103	161	85.5	232	199	84.5	14.0	14.4
Co	20.4	32.6	34.4	19.8	40.9	42.3	20.0	16.1	15.7
Ni	2.79	51.5	62.8	60.7	110	105	54.1	16.1	12.8
Ga	20.9	22.0	22.6	22.6	21.0	21.6	22.4	18.3	18.6
Rb	50.3	37.6	36.8	21.3	25.2	31.2	29.9	60.3	55.6
Sr	708	668	644	1191	1011	998	1194	892	920
Y	36.5	33.6	35.8	20.4	28.1	29.2	19.4	14.0	14.7
Zr	259	285	305	172	268	277	162	129	112
Nb	7.48	29.1	31.4	5.86	7.94	7.841	5.70	5.14	4.95
Cs	15.3	4.12	28.6	2.58	2.85	3.55	3.63	20.4	20.4
Ba	592	616	638	878	552	618	645	764	842
Hf	6.94	7.02	7.20	4.35	6.73	6.86	4.02	3.75	3.27
Ta	0.51	1.88	2.00	0.34	0.45	0.48	0.32	0.41	0.38
Pb	6.53	7.94	8.14	7.91	7.85	7.75	7.42	8.53	8.43
Th	3.19	2.95	2.84	2.06	2.03	2.89	1.86	8.46	7.99
U	1.13	0.83	0.83	0.74	0.85	0.99	0.67	2.67	2.57
La	22.6	37.9	39.7	25.9	29.2	27.4	25.3	20.0	20.5
Ce	55.0	83.0	87.6	57.1	67.4	61.3	55.5	43.4	43.8
Pr	8.31	10.8	11.5	7.41	9.06	8.95	7.14	5.435	5.59
Nd	36.4	43.6	46.8	29.6	37.1	35.1	28.5	21.5	21.5
Sm	9.18	9.41	10.1	5.87	8.00	8.52	5.92	4.28	4.26
Eu	2.55	2.41	2.55	1.72	2.26	2.32	1.71	1.16	1.18
Gd	8.18	8.91	9.57	5.01	7.16	8.02	5.03	3.55	3.68
Tb	1.32	1.29	1.38	0.72	1.00	1.11	0.68	0.52	0.53
Dy	7.64	7.31	7.81	4.03	5.77	6.22	3.76	2.88	2.92
Ho	1.47	1.39	1.48	0.77	1.11	1.13	0.73	0.57	0.58
Er	4.21	3.46	3.74	2.06	2.94	3.21	1.93	1.58	1.55
Tm	0.62	0.48	0.52	0.30	0.42	0.46	0.29	0.25	0.24
Yb	4.05	3.08	3.32	1.99	2.73	3.24	1.85	1.65	1.58
Lu	0.62	0.43	0.47	0.29	0.38	0.45	0.27	0.27	0.24
La_N/Yb_N	4.01	8.84	8.59	9.33	7.67	6.07	9.81	8.65	9.35
Eu/Eu*	0.90	0.80	0.79	0.97	0.91	0.86	0.96	0.91	0.91

(*continued*)

Table 2. (*continued*)

Sample:	BY04-1	BY04-4	BY04-5	BY04-8	SN07-7	SN07-22	SN07-25	SN07-38	BY04-37	BY04-38
Rock type:	R	R	R	R	R	R	R	R	R	R
SiO_2	71.00	70.33	70.74	70.37	71.95	71.65	71.96	70.53	72.45	71.09
TiO_2	0.46	0.44	0.45	0.47	0.34	0.46	0.44	0.47	0.20	0.39
Al_2O_3	14.39	14.28	14.41	15.42	14.40	13.81	13.78	15.32	13.89	14.15
$Fe_2O_3^T$	2.47	2.42	2.42	2.65	1.83	2.66	2.58	2.79	2.04	2.47
MnO	0.06	0.06	0.07	0.03	0.04	0.06	0.03	0.01	0.04	0.05
MgO	0.93	0.93	0.90	0.37	0.55	0.18	0.24	0.36	0.35	0.73
CaO	0.85	0.95	1.04	0.34	0.43	0.24	0.28	0.35	0.81	0.86
Na_2O	4.72	4.63	4.28	5.23	4.85	5.45	5.52	4.51	4.55	4.78
K_2O	4.08	4.06	4.23	4.02	4.35	4.49	4.47	3.54	4.60	3.92
P_2O_5	0.11	0.11	0.11	0.12	0.09	0.09	0.08	0.12	0.04	0.08
LOI	1.22	1.37	1.65	1.32	0.83	0.52	0.61	1.62	0.88	1.43
Total	100.29	99.58	100.3	100.3	99.66	99.62	99.99	99.62	99.85	99.95
Mg-no.	42.7	43.2	42.4	21.7	37.3	11.8	15.6	20.4	25.4	36.9
ASI	1.05	1.04	1.07	1.14	1.07	0.97	0.96	1.29	1.00	1.04
Sc	4.00	4.03	4.07	4.99	4.42	11.5	8.54	6.32	5.43	6.54
V	37.7	37.0	34.9	22.7	35.3	20.8	18.3	19.2	11.0	30.8
Cr	3.58	8.18	5.79	6.10	3.07	1.02	1.11	0.87	3.64	7.80
Co	5.92	5.78	5.92	1.64	3.08	1.18	1.58	1.56	3.32	4.72
Ni	5.50	5.07	5.60	2.89	5.64	3.20	3.42	3.51	2.55	1.66
Ga	12.9	13.0	13.6	19.4	14.4	24.3	25.8	19.1	14.2	14.4
Rb	80.2	75.6	84.0	37.4	129	111	119	102	53.6	89.5
Sr	446	465	572	248	535	61.7	59.4	224	139	81.4
Y	13.7	13.3	12.9	25.3	19.2	54.0	57.6	31.5	26.6	25.1
Zr	184	170	174	273	242	433	456	260	122	209
Nb	5.79	5.72	5.64	10.2	7.61	13.4	12.5	9.93	10.0	9.80
Cs	3.68	3.79	4.68	10.3	8.27	2.55	3.68	17.1	2.65	2.86
Ba	808	787	797	943	923	1065	895	903	901	499
Hf	4.22	4.49	4.29	7.57	6.42	11.1	12.0	7.17	3.96	6.07
Ta	0.55	0.55	0.54	0.80	0.66	1.02	0.98	0.70	0.87	0.87
Pb	11.3	11.1	12.4	18.2	16.3	23.5	21.5	15.5	10.7	13.3
Th	6.64	6.62	6.56	11.14	8.91	13.5	14.1	11.2	11.3	11.3
U	1.86	1.87	1.85	2.72	2.25	1.66	2.13	2.48	2.40	2.81
La	17.6	17.4	16.5	26.6	27.6	73.6	65.2	41.9	26.4	21.0
Ce	35.6	35.7	36.7	68.3	55.6	151	139	83.5	45.2	39.2
Pr	4.37	4.27	4.08	6.81	6.40	19.3	16.4	10.9	5.88	4.60
Nd	15.8	15.3	14.7	26.94	22.0	73.7	68.6	41.1	22.3	17.4
Sm	3.19	3.07	2.88	5.62	4.12	13.8	11.5	7.83	4.46	3.60
Eu	0.88	0.80	0.82	1.32	0.91	2.93	2.88	1.72	0.95	0.77
Gd	2.83	2.52	2.62	5.24	3.72	12.6	12.2	7.01	4.49	3.62
Tb	0.48	0.43	0.46	0.86	0.57	1.86	1.82	1.02	0.77	0.64
Dy	2.68	2.46	2.52	4.92	3.47	11.2	10.9	5.71	4.98	4.25
Ho	0.56	0.49	0.51	1.02	0.70	2.30	2.55	1.19	1.04	0.93
Er	1.64	1.46	1.51	3.12	2.02	6.27	7.31	3.33	3.05	2.67
Tm	0.27	0.25	0.26	0.49	0.35	0.95	1.05	0.51	0.47	0.42
Yb	1.76	1.72	1.68	3.23	2.43	6.53	6.61	3.22	3.19	2.71
Lu	0.29	0.26	0.27	0.54	0.38	0.97	1.01	0.51	0.49	0.44
La_N/Yb_N	7.19	7.28	7.07	5.90	8.14	8.09	7.08	9.32	5.93	5.54
Eu/Eu*	0.90	0.88	0.91	0.75	0.71	0.68	0.74	0.71	0.65	0.65

B, basalt; BA, basaltic andesite; A, andesite; R, rhyolite.

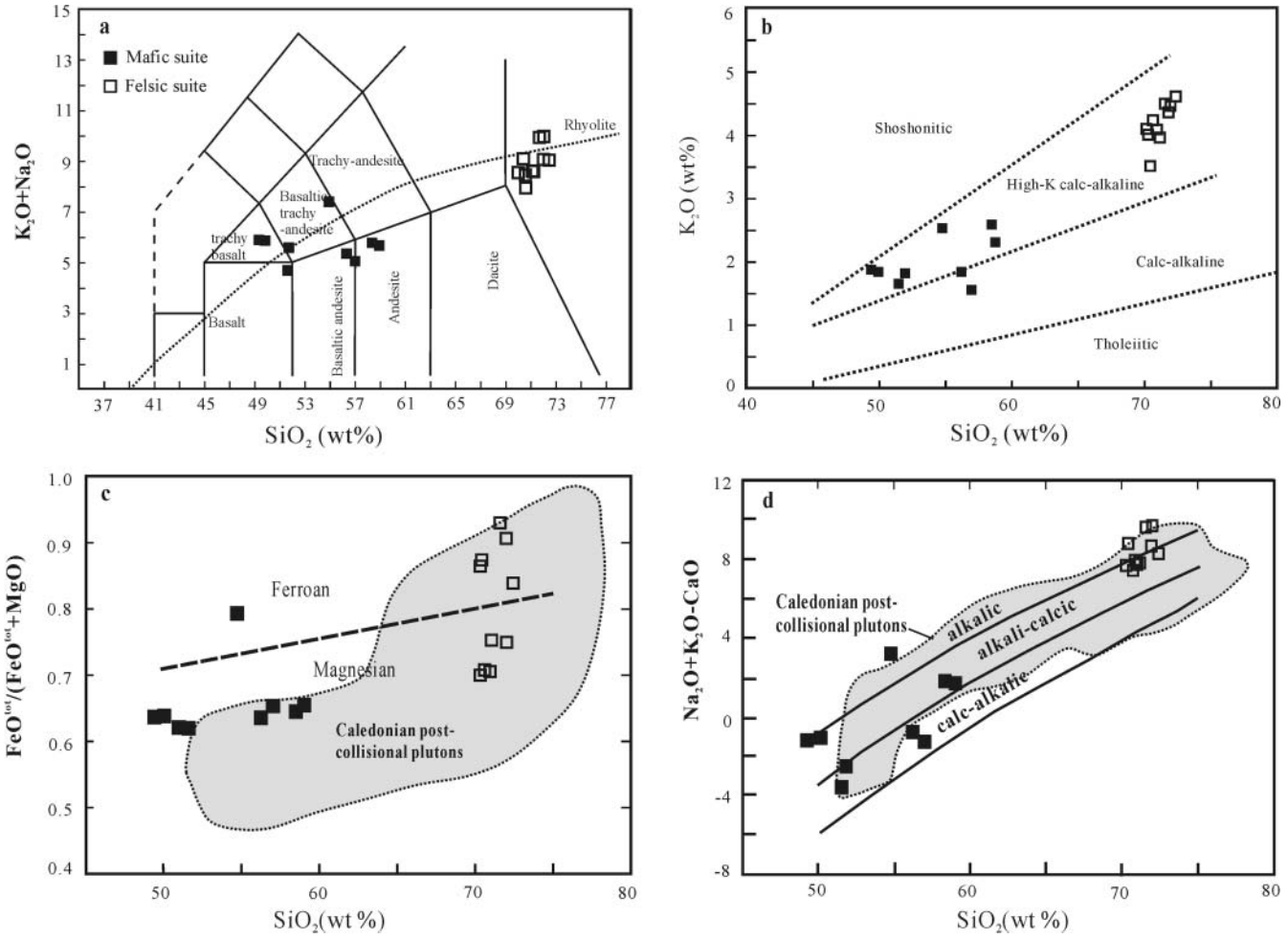

Fig. 3. Classification diagrams for the Sonidzuoqi volcanic rocks. (**a**) Plot of total alkalis v. silica (Le Maitre 1989). (**b**) Plot of K_2O v. SiO_2. Field boundaries after Peccerillo & Taylor (1976). (**c**) Plot of $FeO_t/(FeO_t + MgO)$ v. SiO_2 (Frost *et al.* 2001*b*). (**d**) Plot of $(Na_2O + K_2O - CaO)$ v. SiO_2 (Frost *et al.* 2001*b*). The field for Caledonian post-collisional plutons in (**c**) and (**d**) is based on the data compilation of Frost *et al.* (2001*b*).

Sr–Nd–Pb isotopic compositions

The whole-rock Sr–Nd–Pb isotope data are presented in Tables 3 and 4. Initial isotopic ratios were calculated based on the zircon U–Pb ages of 289 Ma and 287 Ma for the mafic and felsic samples, respectively. The mafic rocks have initial $^{87}Sr/^{86}Sr$ ratios of 0.7037–0.7042 and strongly positive $\varepsilon_{Nd}(t)$ of +3.79 to +6.80 (Fig. 5). They also have moderately positive $\Delta 8/4$ $\{[(^{208}Pb/^{204}Pb)_i - (^{208}Pb/^{204}Pb)_{NHRL}] \times 100 = 17.2–42.5\}$ and moderately high $\Delta 7/4$ $\{[(^{207}Pb/^{204}Pb)_I - (^{207}Pb/^{204}Pb)_{NHRL}] \times 100 = 3.55–6.54\}$ values with $^{206}Pb/^{204}Pb_i = 17.94–18.11$, $^{207}Pb/^{204}Pb_i = 15.47–15.51$, and $^{208}Pb/^{204}Pb_i = 37.61–37.90$. In the $^{207}Pb/^{204}Pb_i$ and $^{208}Pb/^{204}Pb_i$ v. $^{206}Pb/^{204}Pb_i$ correlation plots (Fig. 6a and b), they plot well above the Northern Hemisphere Reference Line (NHRL, Zindler & Hart 1986) and also lie within Indian mid-ocean ridge basalt (I-MORB) and OIB fields.

The rhyolites have initial $^{87}Sr/^{86}Sr$ ratios of 0.7035–0.7038, positive $\varepsilon_{Nd}(t)$ values of +5.43 to +6.05 (Fig. 5) and high initial $^{206}Pb/^{204}Pb$ ratios of 18.02–18.15. In the $^{207}Pb/^{204}Pb_i$ and $^{208}Pb/^{204}Pb_i$ v. $^{206}Pb/^{204}Pb_i$ correlation plots (Fig. 6a and b), they also plot above the NHRL, overlapping with basalt fields.

Discussion

Origin of the mafic rocks

With the exception of two andesite samples showing relatively high (>4%) loss on ignition (LOI), most mafic samples display relatively low LOI. This, together with consistent variations of both immobile and mobile elements on the primitive mantle-normalized patterns and constricted Sr–Nd isotopic compositions of the mafic rocks, suggests that they have undergone insignificant post-eruption alteration. Therefore, we believe that the elemental variations in these samples could be ascribed to original magmatic processes and can be used for characterizing the magma source of these rocks.

The basaltic and basaltic andesite samples show relatively higher concentrations of MgO (up to 5.8%) and Fe_2O_3* (6.7–11.4%) and lower silica contents (SiO_2 = 49.4–56.9%) than those of any crustal materials (Rudnick & Gao 2003) or crust-derived melts (e.g. Patiño Douce & McCarthy 1997), clearly arguing for a mantle source. However, their Mg-number (50–52), and Cr and Ni abundances are not elevated enough for them to be qualified as primary mantle melts. Instead, these rocks may

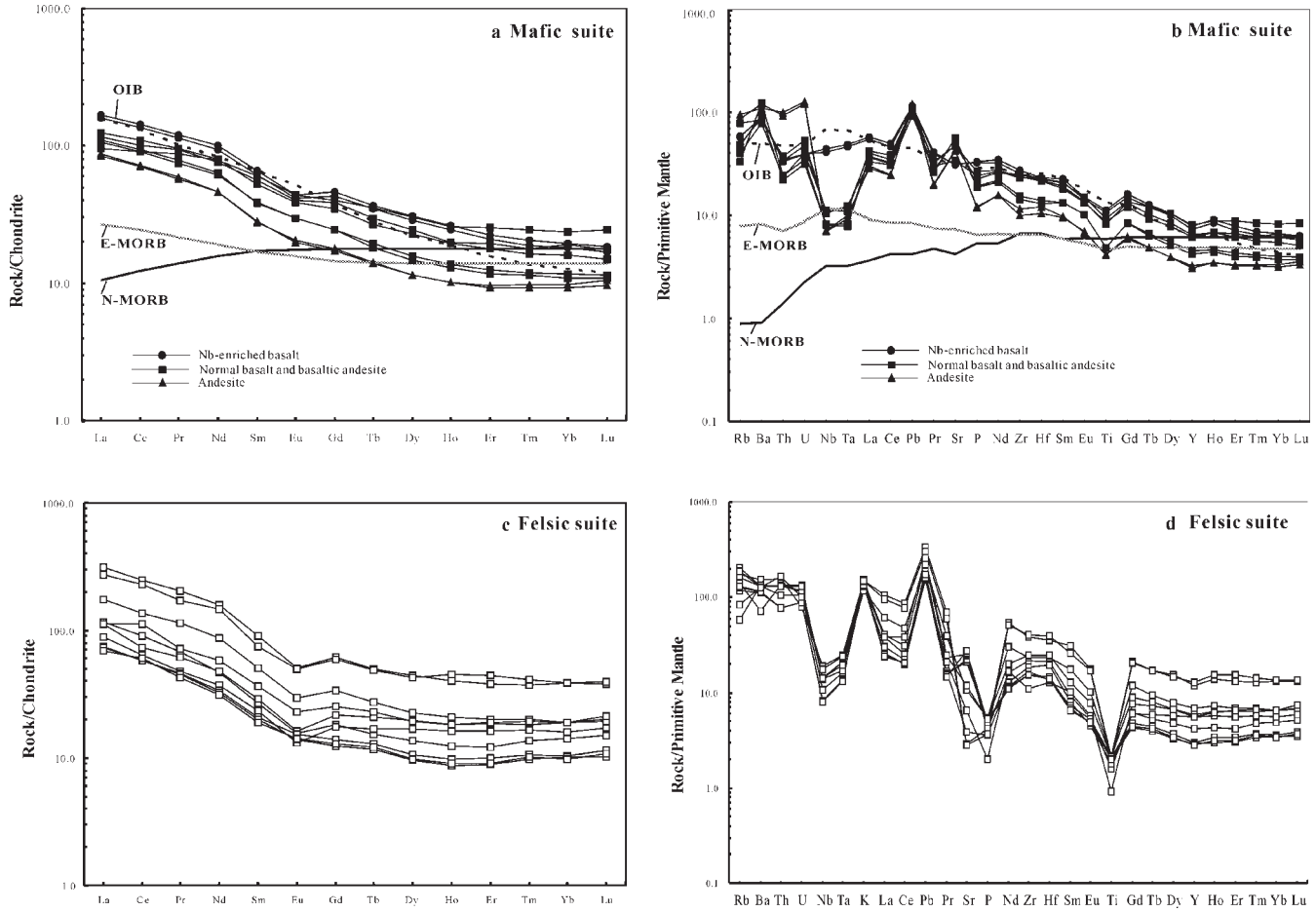

Fig. 4. Chondrite-normalized REE patterns (**a**, c) and primitive mantle-normalized trace element spidergrams (**b**, **d**) for the mafic and felsic suites from the Sonidzuoqi volcanic rocks. Normalization values are from Sun & McDonough (1989). The data for oceanic island basalt (OIB), normal mid-ocean ridge basalt (N-MORB) and enriched mid-ocean ridge basalt (E-MORB) are also from Sun & McDonough (1989).

represent residual liquids that have undergone some crystal fractionation, most probably of olivine and pyroxene, from a more magnesium-rich parental magma either in magma chambers or en route to the surface. This is consistent with the presence of olivine and pyroxene as dominant phenocrysts in the mafic rocks.

Among conceivable mantle sources, the asthenosphere is distinct from the lithospheric mantle by its different rheology and evolutionary history. The former is generally hot and convective, and has a depleted or primitive mantle character in both chemical and isotopic compositions owing to the circulation of incipient melts from low degrees of melting, whereas the latter is cold and conductive with enriched isotopic compositions because of its long isolation from the convective mantle and interaction with magmas. In our case, as is specifically demonstrated by the Late Carboniferous gabbroic diorites ($^{87}Sr/^{86}Sr_i \approx 0.7052$, $\varepsilon_{Nd}(t) \approx +2.4$) from Sonidzuoqi (Chen *et al.* 2000) and numerous mafic–ultramafic complexes from the neighbouring regions (Wu *et al.* 2004; Zhang *et al.* 2010*a*), the lithospheric melts from this orogenic belt seem to have a more enriched isotopic composition and Neo- to Mesoproterozoic Nd model ages (mainly 0.78–1.25 Ga). On the other hand, the asthenospheric melts as represented by the early Permian Xilinhot tholeiitic lavas have a highly

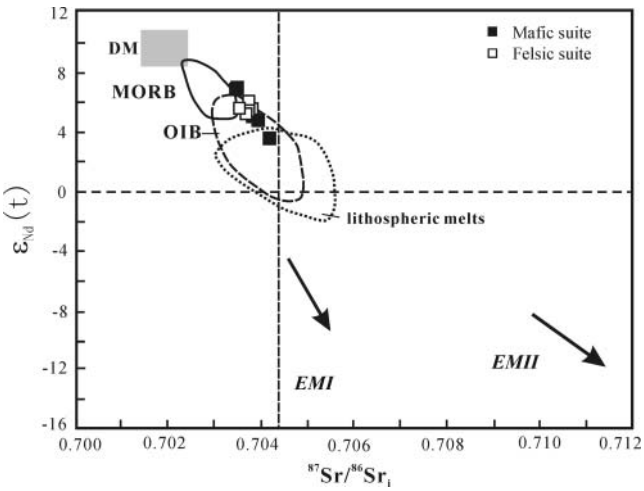

Fig. 5. Plot of initial $\varepsilon_{Nd}(t)$ and $^{87}Sr/^{86}S_i$ for the Sonidzuoqi volcanic rocks. DM, depleted mantle source; EMI and EMII, enriched mantle I and II sources; fields for DM, MORB and OIB are from Zindler & Hart (1986). Field for regional lithospheric melts is based on the data from Chen *et al.* (2000), Wu *et al.* (2004) and Zhang *et al.* (2010*a*).

Table 3. *Rb–Sr and Sm–Nd isotopic compositions for the Sonidzuoqi volcanic rocks*

Sample number	Rb (ppm)	Sr (ppm)	$^{87}Rb/^{86}Sr$	$^{87}Sr/^{86}Sr$	$\pm2\sigma$	$^{87}Sr/^{86}Sr_i$	Sm	Nd	$^{147}Sm/^{144}Nd$	$^{143}Nd/^{144}Nd$	$\pm2\sigma$	Initial Nd	$\varepsilon_{Nd}(t)$	T_{DM} (Ma)
Mafic rocks														
BY04-2	47.16	725.4	0.1882	0.704424	15	0.703728	8.294	35.1	0.1432	0.51290	13	0.51265	6.79	552
BY04-14	31.7	631.8	0.1450	0.70477	15	0.704178	8.93	42.1	0.1283	0.51270	15	0.51246	3.79	796
SN07-2	19.9	939.4	0.0614	0.70401	13	0.703759	6.72	33.3	0.1220	0.51285	14	0.51262	6.80	506
SN07-10	23.8	1086	0.0635	0.70418	12	0.703921	5.01	26.1	0.1160	0.51273	15	0.51251	4.67	662
SN07-30	56.0	872.2	0.1856	0.70455	12	0.70379	3.96	20.1	0.1190	0.51275	12	0.51253	5.01	646
Felsic rocks;														
BY04-1	78.04	449.9	0.5003	0.70564	14	0.703792	2.84	14.7	0.1167	0.51280	14	0.512604	5.87	546
BY04-4	79.1	476.2	0.4793	0.70551	10	0.703734	2.82	14.4	0.1184	0.51282	14	0.512614	6.05	537
BY04-5	83.71	581.3	0.4151	0.70537	15	0.703772	2.70	14.0	0.1168	0.51280	12	0.512600	5.79	553
SN07-7	113.9	488.7	0.6748	0.70644	13	0.703684	4.23	23.9	0.1071	0.51275	16	0.512547	5.43	576
SN07-22	98.9	44.7	6.4144	0.72973	13	0.70353	14.6	85.4	0.1037	0.51276	12	0.512566	5.81	540

$^{87}Sr/^{86}Sr_{ir} = (^{87}Sr/^{86}Sr)_{sample} - (^{87}Rb/^{86}Sr)_{sample} \times (e^{\lambda t} - 1)$, $\lambda = 1.42 \times 10^{-11}$ a^{-1} (Steiger & Jäger 1977); initial $Nd = (^{143}Nd/^{144}Nd)_{sample} - (^{147}Sm/^{144}Nd)_{sample} \times (e^{\lambda t} - 1)$, $\varepsilon_{Nd} = [(^{143}Nd/^{144}Nd)_{sample}/(^{143}Nd/^{144}Nd)_{CHUR} - 1] \times 10000$, $f_{Sm/Nd} = (^{147}Sm/^{144}Sm)_{sample}/(^{147}Sm/^{144}Sm)_{CHUR} - 1$, $T_{DM} = 1/\lambda \times \ln\{1 + [(^{143}Nd/^{144}Nd)_{sample} - 0.51315]/[(^{147}Sm/^{144}Nd)_{sample} - 0.2137]\}$, where $(^{147}Sm/^{144}Nd)_{CHUR} = 0.1967$, $(^{143}Nd/^{144}Nd)_{CHUR} = 0.512638$, $\lambda_{SM} = 6.54 \times 10^{-12}$ a^{-1} (Lugmair & Marti 1978).

Table 4. *Pb isotopic compositions for the Sonidzuoqi volcanic rocks*

Sample	U	Th	Pb	$^{206}Pb/^{204}Pb$	$^{207}Pb/^{204}Pb$	$^{208}Pb/^{204}Pb$	$^{238}U/^{204}Pb$	$^{235}U/^{204}Pb$	$^{232}Th/^{204}Pb$	$(^{206}Pb/^{204}Pb)_i$	$(^{207}Pb/^{204}Pb)_i$	$(^{208}Pb/^{204}Pb)_i$	$\Delta7/4$	$\Delta8/4$
Mafic rocks														
BY04-2	1.13	3.19	6.53	18.386	15.494	38.019	10.91	0.08	31.81	17.937	15.471	37.607	3.55	29.4
BY04-14	0.832	2.954	7.935	18.373	15.531	38.248	6.63	0.05	24.33	18.071	15.513	37.900	6.54	42.5
SN07-2	0.839	2.034	7.849	18.272	15.510	37.974	6.72	0.05	16.84	17.966	15.494	37.733	5.56	38.5
SN07-10	0.671	1.855	7.419	18.237	15.510	37.967	5.69	0.04	16.24	17.976	15.496	37.733	5.68	37.3
SN07-30	2.674	8.457	8.533	19.028	15.550	38.635	20.1	0.15	65.7	18.106	15.502	37.689	4.83	17.2
Felsic rocks														
BY04-1	1.86	6.64	11.29	18.509	15.492	38.113	10.41	0.08	38.41	18.08	15.47	37.616	1.9	13
BY04-4	1.87	6.62	11.06	18.540	15.536	38.256	10.72	0.08	39.21	18.099	15.513	37.748	6.04	24
BY04-5	1.85	6.56	12.37	18.486	15.513	38.156	9.46	0.07	34.65	18.097	15.493	37.707	4.03	20.1
SN07-7	2.253	8.912	16.26	18.423	15.524	38.203	8.76	0.06	35.82	18.024	15.503	37.691	5.84	27.3
SN07-22	1.66	13.50	23.49	18.356	15.524	38.237	4.47	0.03	37.52	18.153	15.513	37.700	5.47	12.7

$\lambda_{U238} = 1.55125 \times 10^{-10}$ a^{-1}; $\lambda_{U235} = 9.8485 \times 10^{-10}$ a^{-1}; $\lambda_{Th232} = 4.9475 \times 10^{-11}$ a^{-1} (Steiger & Jäger 1977). $\Delta7/4 = [(^{207}Pb/^{204}Pb)_I - (^{207}Pb/^{204}Pb)_{NHRL}] \times 100$; $\Delta8/4 = [(^{208}Pb/^{204}Pb)_i - (^{208}Pb/^{204}Pb)_{NHRL}] \times 100$; $(^{207}Pb/^{204}Pb)_{NHRL} = 0.1084 \times (^{206}Pb/^{204}Pb)_i + 13.491$ (Hart 1984); $(^{208}Pb/^{204}Pb)_{NHRL} = 1.209 \times (^{206}Pb/^{204}Pb)_i + 15.627$ (Hart 1984).

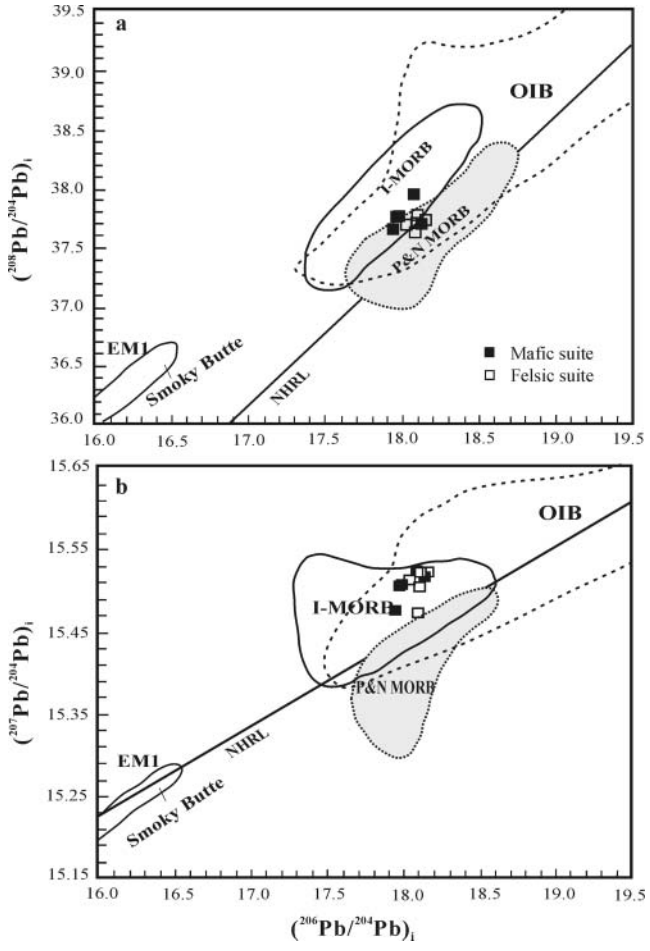

Fig. 6. Initial $^{206}Pb/^{204}Pb$ v. $^{208}Pb/^{204}Pb$ and $^{207}Pb/^{204}Pb$ for the Sonidzuoqi volcanic rocks. Fields for I-MORB (Indian MORB), P&N MORB (Pacific and North Atlantic MORB) and OIB are from Barry & Kent (1998) and Hoffman (2003); NHRL (Northern Hemisphere Reference Line) from Zindler & Hart (1986); Smoky Butte lamprophyres from Fraser *et al.* (1985). MORB, mid-oceanic ridge basalt; OIB, oceanic island basalt; EMI, enriched mantle I.

depleted isotopic composition ($^{87}Sr/^{86}Sr_i \approx 0.703–0.705$, $\varepsilon_{Nd}(t) \approx +6.9$ to $+8.0$) and younger Nd model ages ($T_{DM} = 0.39–0.56$ Ga) (Zhang *et al.* 2008) that are consistent with the Middle–Late Paleozoic ophiolites in the region (Miao *et al.* 2007; Jian *et al.* 2008).

As shown above, our mafic rocks exhibit distinctive elemental and isotopic characteristics. Two basalt samples show high contents of TiO_2 and P_2O_5, elevated HFSE, low La/Nb and high La/Ba ratios, OIB-like Sr–Nd–Pb isotopic composition and Neoproterozoic Nd model age (0.8 Ga). Such Nb-enriched basalts are generally thought to be derived from the partial melting of the slab melt–metasomatized mantle wedge peridotite (Sajona *et al.* 1996; Aguillón-Robles *et al.* 2001; Wang *et al.* 2007). This general origin seems to be compatible with the geochemical characteristics of these Nb-enriched basalts.

In contrast, the majority of our mafic rocks exhibit a more depleted isotopic composition ($^{87}Sr/^{86}Sr_i = 0.7037–0.7039$, $\varepsilon_{Nd}(t) = +4.67$ to $+6.79$, $^{206}Pb/^{204}Pb_i = 17.94–18.11$) that is consistent with a MORB-like asthenospheric component. Furthermore, the selective enrichment of LILE and LREE over HFSE in these samples leads to high La/Nb (3.0–4.4), Ba/Nb (69–149), and Zr/Nb ratios (28–34), and low La/Ba and Ce/Pb (7.2–8.6), comparable with those of arc volcanic rocks worldwide (e.g. Stern 2002). In general, such geochemical features can be attributed either to partial melting of a mantle source that was previously enriched in LILE and LREE by distinct metasomatic agents (e.g. fluid, silicic or carbonatite melt) prior to magma generation, or to extensive crustal contamination of MORB (or OIB)-like melts during magma emplacement.

For these rocks, their relatively primitive Sr–Nd isotopic compositions and the lack of any systematic correlated variations of $^{87}Sr/^{86}Sr_i$ and $\varepsilon_{Nd}(t)$ with SiO_2 (Fig. 7) exclude crustal contamination from having played any significant role in their genesis. Moreover, crustal assimilation during emplacement would result in more variable contamination in the case of sedimentary rocks or more uniform contamination in the case of continental crust, but not the coupled enrichment in more mobile highly incompatible lithophile elements (e.g. U) and negative Nb–Ta–Ti anomalies (Zhou *et al.* 2004). In addition, unimodal zircon age populations provide another piece of evidence that there was very little crustal contamination. As such, we attribute these geochemical signatures to metasomatism induced by the fluids or silicate melts released from a descending and dehydrating slab during the earlier subduction of the Palaeo-Asian Ocean.

With these distinctive subduction-related trace elemental and MORB-like isotopic characters, the mafic rocks are reminiscent of numerous coeval and modern analogues, such as the Early Permian Karamay mafic intrusions from the West Junggar fold belt of NW China (Chen & Arakawa 2005), the mafic lavas from

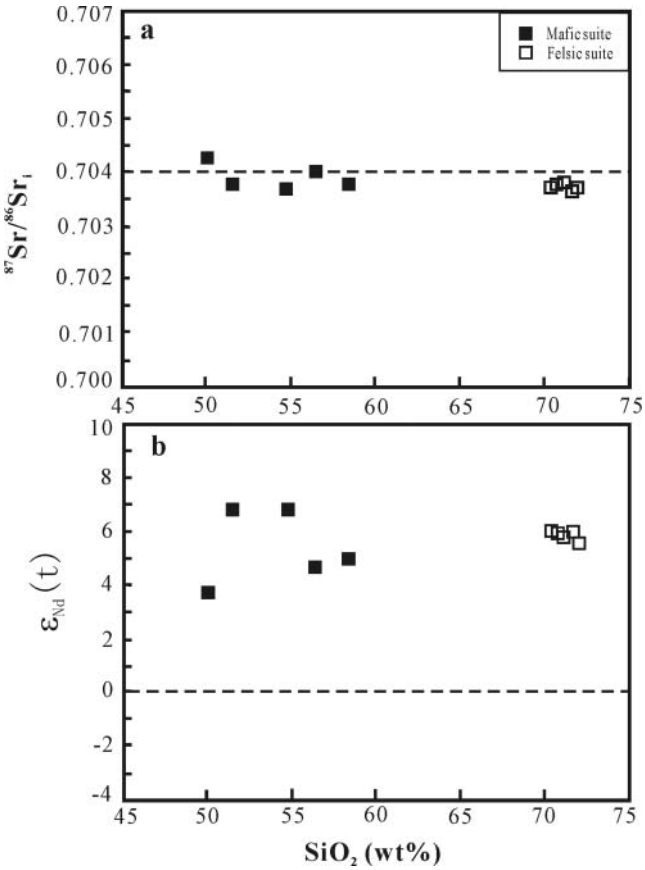

Fig. 7. Plots of (**a**) $^{87}Sr/^{86}S_i$ v. SiO_2 and (**b**) $\varepsilon_{Nd}(t)$ v. SiO_2.

the North Anatolian Block of northwestern Turkey (Kürkcüoğlu *et al.* 2008) and the high-K calc-alkaline basalts from the Northern Taiwan Volcanic Zone (Wang *et al.* 2004). All of these analogues are interpreted to have an origin consistent with partial melting of a metasomatized asthenospheric mantle within a post-subduction tectonic regime (Wang *et al.* 2004; Chen & Arakawa 2005; Kürkcüoğlu *et al.* 2008).

Tectonic affiliation of mafic rocks with a within-plate setting is also evident on some discrimination diagrams. For instance, many mafic samples have high Ti/V (50–100) typical of within-plate basalt (Fig. 8a). All the samples narrowly plot in the field of within-plate basalt on both the Zr/Y–Zr plot of Pearce & Norry (1979) (Fig. 8b) and the Ti–Zr–Y plot of Pearce & Cann (1973) (Fig. 8c). Therefore, we suggest that two distinctive mantle sources (i.e. one a fluid-metasomatized asthenospheric mantle component and the other a fluid-metasomatized lithospheric component) were involved in the generation of the Sonidzuoqi mafic volcanic rocks, possibly in a within-plate extensional regime.

Petrogenesis of the felsic rocks

As with the mafic rocks, most felsic samples show low LOI and consistent trace elemental variations on the primitive mantle-normalized diagrams indicative of insignificant post-eruption alteration. This makes it feasible for the elemental variations in these samples to fingerprint their magma sources.

As shown above, most felsic samples have high alkali contents, low CaO and P_2O_5, small negative Eu anomalies, elevated Ba and Sr, and low abundances of Nb, Ta and Ti. These are typical of major and trace element geochemical features of undifferentiated I-type magmas (Landenberger & Collins 1996), but not S-type magmas (Clemens 2003). Specifically, these rocks plot mostly in the field of A-type granite in the $K_2O + Na_2O$ v. Ga/Al diagram of Whalen *et al.* (1987) (Fig. 9a) but mainly in the fields of M-, I- and S-types in the FeO*/MgO and Nb v. Ga/Al diagrams of Whalen *et al.* (1987) (Fig. 9b and c). In the FeO*/MgO and $(K_2O + Na_2O)$/CaO v. (Zr + Nb + Ce + Y) diagrams of Whalen *et al.* (1987) (Fig. 9d and e), most samples straddle the fields between unfractionated I- and A-type granite. Furthermore, their compositional trends bear a close resemblance to that of Caledonian-type post-collisional granites of Britain in the MALI v. SiO_2 diagram of Frost *et al.* (2001*b*) (Fig. 3c and d). This is also consistent with their distribution in the Rb v. Y + Nb diagram of Pearce *et al.* (1984). As shown in Figure 9f, the felsic rocks mainly plot in the field of volcanic arc granite but mostly also plot in the post-collisional field of Pearce (1996). Such ambiguities are typical for post-collisional granitoid suites in general (Pearce 1996), and suggest a transition from calc-alkaline to alkaline magmatic series in orogenic to post-orogenic tectonic settings (Barbarin 1999). Therefore, the Sonidzuoqi felsic volcanic rocks can be described as a post-collisional alkaline-calcic to alkaline I-type suite.

Multiple petrogenetic models have been proposed for the origins of such felsic magmas, including: (1) crustal assimilation and fractional crystallization (AFC) of mantle-derived basaltic magma (Moghazi 2003; Chen & Arakawa 2005; Sisson *et al.* 2005); (2) partial melting of K-rich meta-andesitic to basaltic protoliths under crustal conditions (Roberts & Clemens 1993; Borg & Clynne 1998; Altherr *et al.* 2000; Roberts *et al.* 2000; Ferré & Leake 2001; Sisson *et al.* 2005; Guo *et al.* 2009; Topuz *et al.* 2010; Zhang *et al.* 2010*a*); (3) hybridization between mantle-derived and crustal magmas (Küster & Harms 1998; Clemens *et al.* 2009).

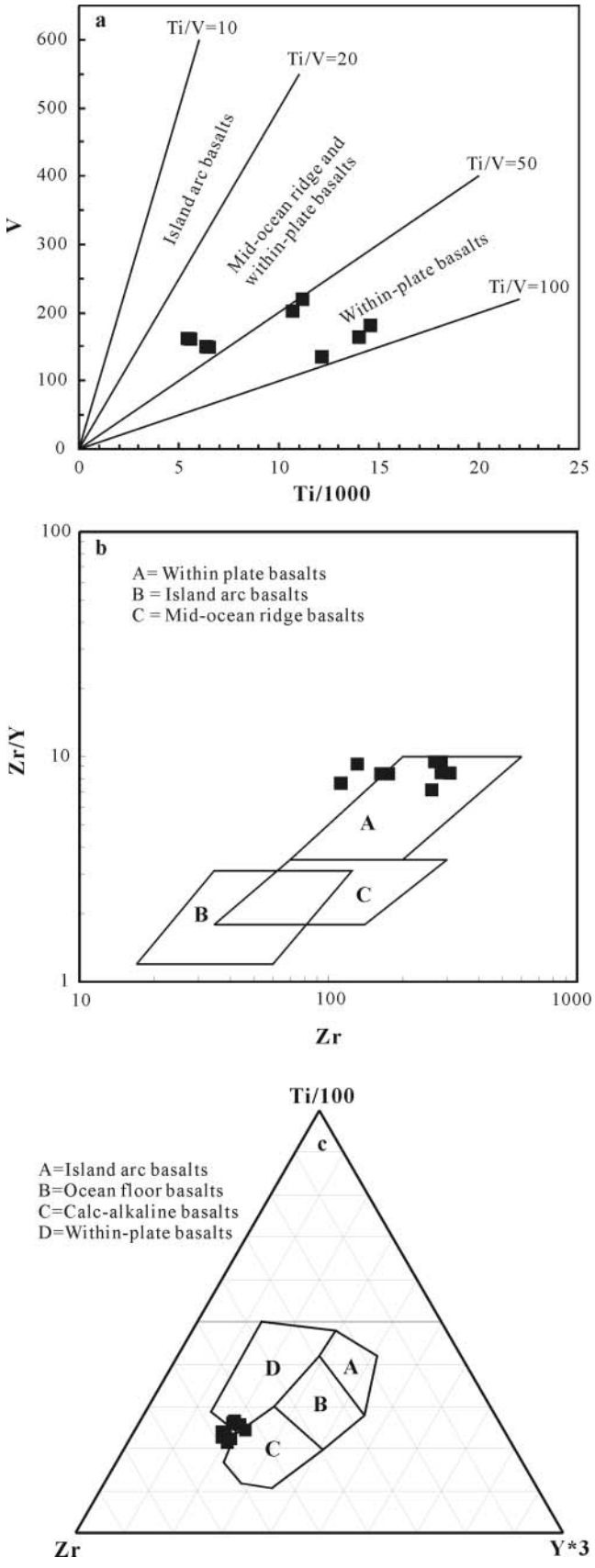

Fig. 8. (**a**) V v. Ti/1000 (Shervais 1982), (**b**) Zr v. Zr/Y (Pearce & Norry 1979), and (**c**) Ti–Zr–Y (Pearce & Cann 1973) plots for the mafic suite from the Sonidzuoqi volcanic rocks.

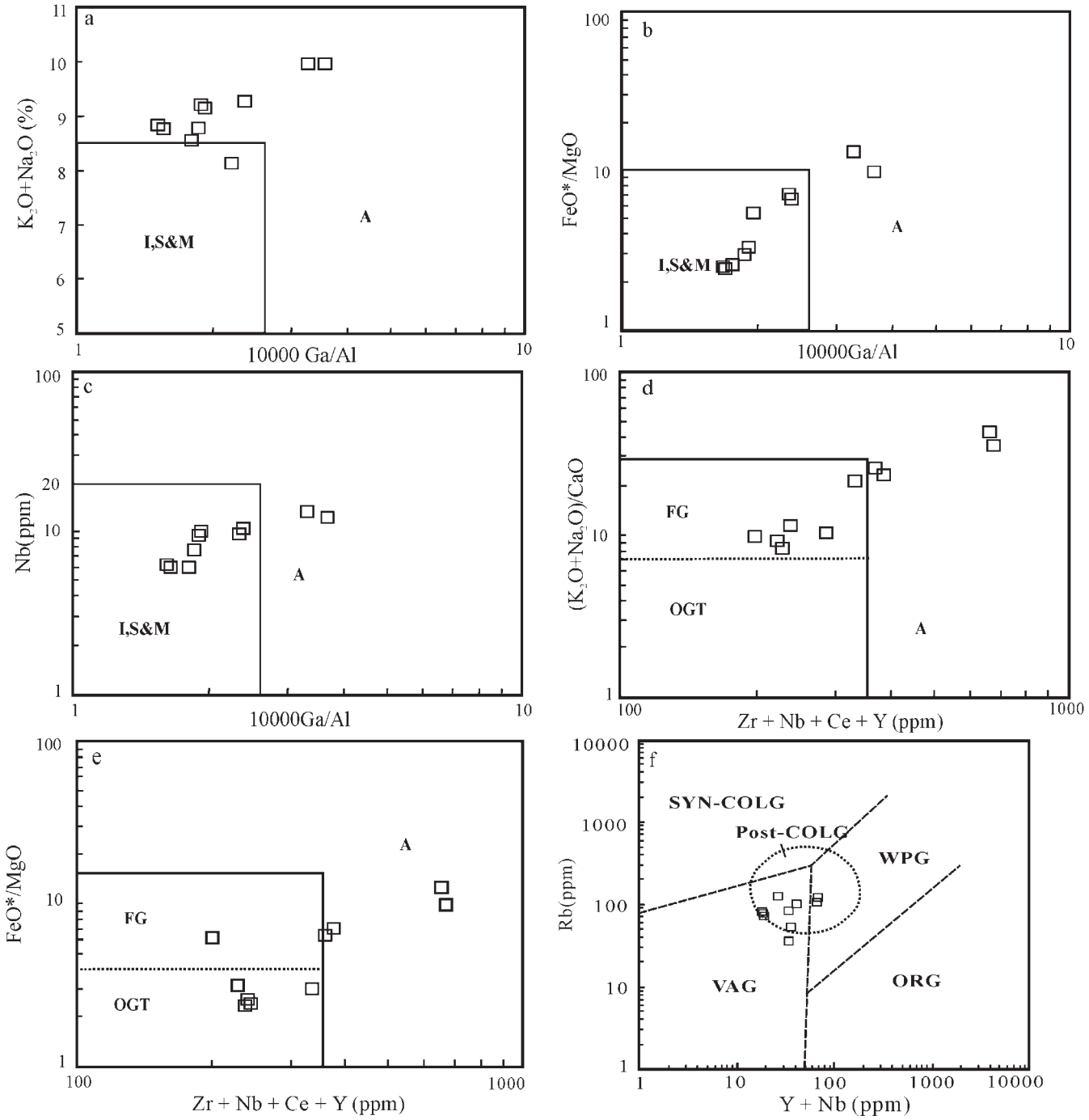

Fig. 9. (**a**–**c**) $K_2O + Na_2O$, FeO*/MgO and Nb v. 10 000 Ga/Al discrimination diagrams of Whalen *et al.* (1987), I, S & M are I-, S- and M-type granites. (**d**, **e**) $(K_2O + Na_2O)/CaO$ and FeO*/MgO v. (Zr + Nb + Ce + Y) discrimination diagrams of Whalen *et al.* (1987). FG, fractionated felsic granites; OGT, unfractionated I-, S- and M-type granites. (**f**) Rb v. Y + Nb tectonic discrimination diagram of Pearce *et al.* (1984) and Pearce (1996). FeO* = Fe_2O_3* × 0.9; VAG, volcanic arc granites; WPG, within-plate granites; COLG, collisional granites; ORG, oceanic ridge granites.

Hybridization processes involving magma mixing or crustal assimilation during magma emplacement appear to have been insignificant. To begin with, the considerable overlap of the initial isotope ratios between felsic and mafic rocks is inconsistent with what might be expected in the case of magma mixing and crustal assimilation. Furthermore, undercooled magmatic inclusions and xenocrystic inherited zircons, typical indicators for magma hybridization process (e.g. Bonin 2004), are rarely observed within the felsic rocks.

Given the coexistence of the coeval mantle-derived mafic magmas and the experimental work of Sisson *et al.* (2005) that substantial amounts of high-K felsic magmas could be produced by advanced crystallization–differentiation of medium- to high-K basaltic sources, it is tempting to ascribe our felsic rocks

to a fractional crystallization process. However, several arguments are against this possibility. First, most felsic samples are characterized by Ca/Sr (5.7–14), Rb/Sr (0.15–0.24), Rb/Ba (0.04–0.18) and K/Ba (23–39) ratios that are comparable with those of the unfractionated parental magmas for I- or A-type rhyolitic melts (Landenberger & Collins 1996; Jung *et al.* 1998). These little fractionated elemental characters, plus their small negative Eu anomalies, seem to rule out an origin by extensive fractional crystallization. Second, the present case lacks a continuum in rock type and composition that is generally expected for a magma differentiation model (Whitaker *et al.* 2008) as in the cases of the high-K calc-alkaline Dokhan volcanic suite (Moghazi 2003) and the high-K calc-alkaline volcanic suite from the northern Tianshan range (Wang *et al.* 2007). The differentiated felsic products in these cases consistently develop chondrite-normalized REE patterns with a concave-upward shape. Third, the majority of our felsic samples plot along a vertical line in the La/Sm v. La diagram (Fig. 10), a feature restricted to the process of partial melting (Allègre & Minster 1978). Nevertheless, fractional crystallization has also played a part in the intra-suite evolution of the felsic rocks, as shown by the distribution of a few samples along a subhorizontal line (Fig. 10).

As has been well documented by numerous case studies (Borg & Clynne 1998; Altherr *et al.* 2000; Roberts *et al.* 2000; Ferré & Leake 2001; Guo *et al.* 2009; Topuz *et al.* 2010; Zhang *et al.* 2010*a*), a K-rich meta-andesitic to basaltic protolith has been consistently proposed for the generation of high-potassium calc-alkaline I-type magmas. Likewise, it seems reasonable to envisage a similar scenario of partial melting of newly underplated basaltic arc crust for the genesis of our felsic rocks, as supported by the following arguments.

First, these rocks share many features with typical arc magmas, including the arc-like REE patterns, LILE enrichment and negative Nb–Ta anomalies in the spidergrams. Second, their highly positive $\varepsilon_{Nd}(t)$ and low $^{87}Sr/^{86}Sr_i$ ratios indicate that juvenile mantle-derived materials must dominate in the source, and their very young Nd model ages (537–576 Ma) suggest their ultimate derivation from an Early Palaeozoic continental lithosphere. Third, recent experimental work has shown that partial melting of underplated arc basaltic rocks could yield geologically important volumes of medium- to high-K felsic magmas at middle to lower crustal pressures (Sisson *et al.* 2005).

Irrespective of the precise nature of the protoliths, an external heat input is a prerequisite for partial melting of the middle to lower crustal rocks to produce felsic magmas. In our case this heat engine is realized by the continuation of basaltic underplating since the Late Carboniferous, as witnessed by the mafic magmas discussed herein and *c.* 280 Ma asthenospheric melts from the neighbouring region (Zhang *et al.* 2008).

Such favourable coupling between newly underplated basaltic protolith and sustained heat input is reminiscent of that of the Triassic I-type granites from the New England Fold belt of eastern Australia (Landenberger & Collins 1996), the Late Permian to Early Triassic high-K calc-alkaline granites in the northern Liaoning Block of north China (Zhang *et al.* 2010*a*) and the Early Cretaceous felsic volcanic rocks from the Hinggan Mountains of NE China (Guo *et al.* 2009). In this scenario, mantle-derived magmatic underplating during post-collisional thermal relaxation and extension provides both continued heat supply and newly mantle-derived material to the base of the lower crust. These primitive magmas differentiate to form gabbros and ferrodiorites and thus constitute juvenile lower crust. The heat supply from further underplating owing to rising asthenosphere during continued rifting is capable of elevating lower crustal temperatures to above 900–950 °C (Huppert & Sparks 1988). This leads to partial remelting of a mixed protolith, which contains the newly underplated basaltic lower crust and old lower crustal materials, to yield parental magma for the I-type felsic rocks with small but significant degrees of isotope heterogeneity.

Such a mixed source character is similar to the two-component source model of Wu *et al.* (2002) for the Phanerozoic granitoids in NE China, which envisions that they were produced by melting of a mixed lithology containing lower crustal material that was underplated by a basaltic magma. We can adopt this model to estimate the proportions of juvenile and ancient crustal components involved in the genesis of our felsic rocks. In the model, the newly underplated mafic crust and the ancient lower crust constitute two major components. Modelling results show that the juvenile component that resulted from mantle-derived magmatic underplating has played an essential role in the genesis of the Sonidzuoqi felsic rocks (Fig. 11a and b).

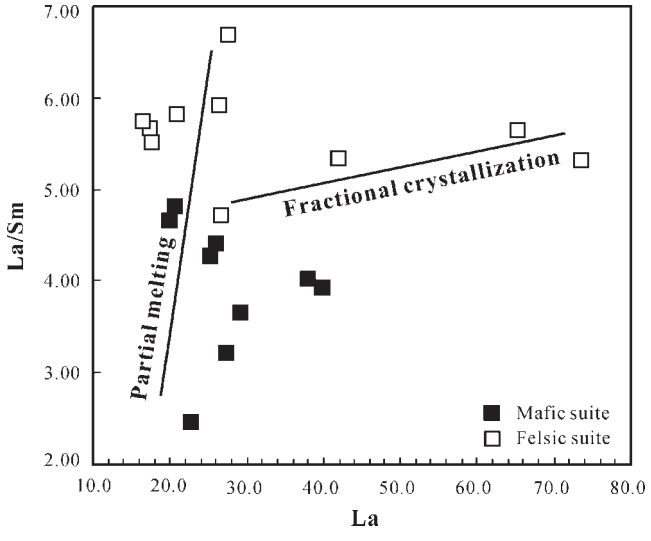

Fig. 10. Plot of La v. La/Sm for the Sonidzuoqi volcanic rocks

Geodynamic implication

Late Palaeozoic palaeogeographical and tectonic reconstructions of the northern China–Mongolia tract indicate that the last domain of the Palaeo-Asian Ocean between the northern and the southern continental blocks existed along the Solonker suture zone (Xiao *et al.* 2003; Shen *et al.* 2006; Jian *et al.* 2010). Current highlighted issues concerning this terminal zone include the evolved tectonic affinity of the opposite-facing continental blocks, subduction polarity and the time of final suture.

Bimodal igneous associations from different geodynamic environments commonly exhibit distinct geochemical affinities and diagnostic mafic–felsic magma relationships (e.g. Pin & Paquette 1997). Post-collisional extensional settings are often typified by coeval medium- to high-K calc-alkaline mafic–felsic igneous suites with contrasting metasomatized mantle and lower crustal sources (Bonin 2004). In our case, this study and previous investigation on the Early Permian mafic igneous rocks from the northern continental block (Zhu *et al.* 2001; Lü *et al.* 2002; Zhang *et al.* 2008) document successive asthenospheric and lithospheric mantle-derived mafic melts. Such dual metasoma-

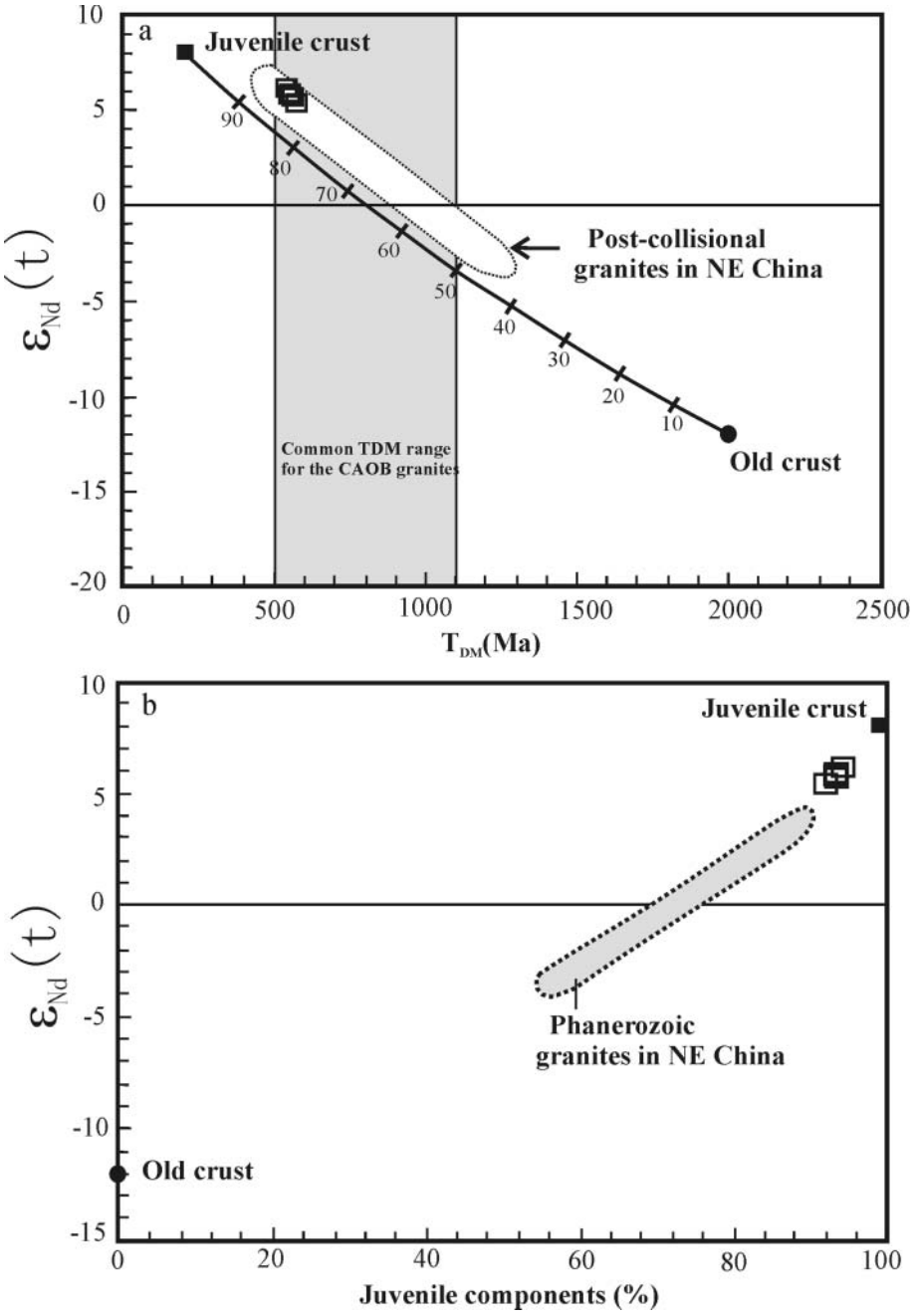

Fig. 11. (**a**) $\varepsilon_{Nd}(t)$ v. T_{DM} diagram for the felsic suite from the Sonidzuoqi volcanic rocks. The field and mixing curve for the post-collisional granites from NE China are from Jahn (2004) and Wu *et al.* (2002); common T_{DM} range for the CAOB (Central Asian Orogenic Belt) granites is from Jahn (2004). (**b**) $\varepsilon_{Nd}(t)$ v. mantle components (%) giving estimated proportions of the juvenile components for the felsic rocks. The equation is $x_m = (Nd_c/Nd_m)/[(Nd_c/Nd_m) + (\varepsilon_m - \varepsilon_s)/(\varepsilon_s - \varepsilon_c)]$ (DePaolo *et al.* 1991), where x_m is per cent juvenile component; Nd_c and Nd_m are Nd concentrations in the crust and mantle components, respectively; ε_m, ε_s and ε_c are Nd isotopic compositions of the mantle or juvenile crust, samples measured and crustal component, respectively. Parameters used are $\varepsilon_m = +8$, $\varepsilon_c = -12$. $Nd_c = 25$ ppm, $Nd_m = 15$ ppm (Wu *et al.* 2003; Jahn 2004).

tized mantle sources can be typically tapped by upwelling of asthenosphere following lithospheric delamination or slab breakoff in a post-subduction extensional regime, such as that of the Neogene volcanism in Algeria (Coulon *et al.* 2002), the Neogene magmatism in northern and southern Tibet (Maheo *et al.* 2002; Williams *et al.* 2004) and the Pliocene magmatism in the Northern Taiwan Mountain belt (Wang *et al.* 2004).

For the felsic rocks, their derivation from a newly underplated lower crust bears close resemblance to numerous counterparts from typical post-collisional igneous associations in many orogenic belts (Altherr *et al.* 2000; Roberts *et al.* 2000; Ferré & Leake 2001; Moghazi 2003; Clemens *et al.* 2009; Topuz *et al.* 2010), which are commonly attributed to decompression following delamination of the lithospheric root or slab breakoff. With these diagnostic signatures, the Sonidzuoqi mafic and felsic volcanic rocks seem to represent a typical bimodal high-K magmatic association developed under a post-collisional extensional regime (Fig. 12).

This typical magmatic association, together with Carboniferous (328–308 Ma) variably foliated calc-alkaline plutonism (Chen *et al.* 2000; Bao *et al.* 2007; Liu *et al.* 2009) and Early Permian (284–274 Ma) bimodal volcanism (Zhang *et al.* 2008) and undeformed A_2-type plutonism (Wu *et al.* 2002; Shi *et al.* 2004), constitute a continuous magmatism developed on a convergent continental margin. The transition in magmatic character reflected the shift in geodynamic regime from an earlier continental arc environment to a later extensional regime. This further suggests that the continental crust was undergoing a

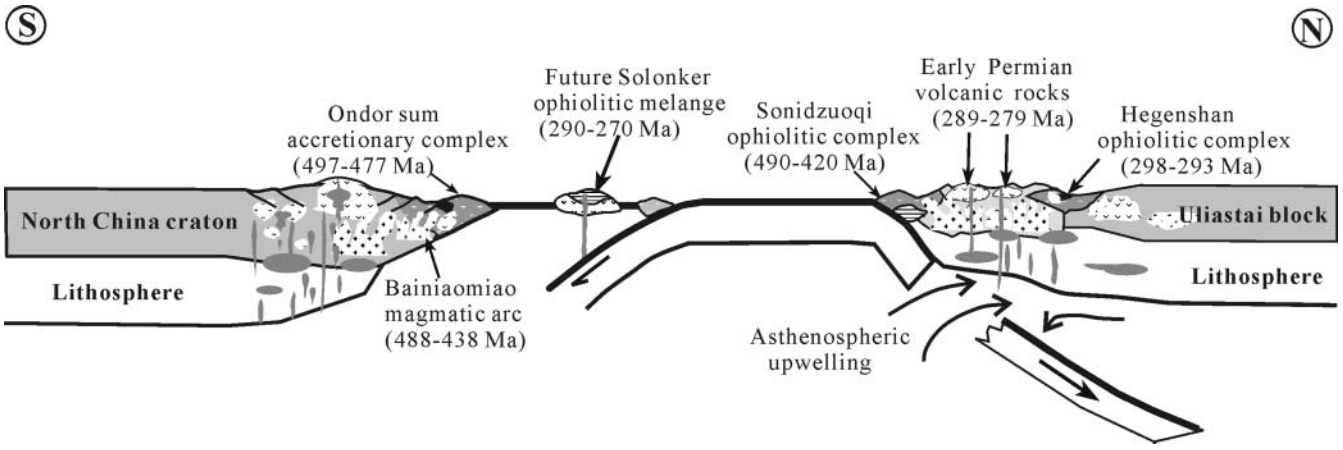

Fig. 12. Schematic illustration of the tectonic setting of the northern China–Mongolia tract when the Sonidzuoqi volcanic rocks erupted.

progressive thinning and can be interpreted as resulting from post-collisional orogenic collapse (Ménard & Molnar 1988).

Southern Mongolia also witnessed a similar transition from Carboniferous island-arc magmatism to Early Permian extension-related magmatism (Blight *et al.* 2010*a*,*b*). The latter, as represented by the Hanbogd alkaline pluton (Kovalenko *et al.* 2006; Yarmolyuk *et al.* 2008), the Mandakh syenite and the North Mandakh peralkaline granite (Blight *et al.* 2010*a*), constitutes a diagnostic A_2-type igneous suite generally found in an extensional environment during post-orogenic stages (Eby 1992). Such consistency in magmatic evolution substantiates the proposition that the northern continental block of northern China is the eastern continuation of the Hutag Uul Block of southern Mongolia.

As documented in various orogenic belts (e.g. Jacobs *et al.* 2008; Goodenough *et al.* 2010) and synthesized by Bonin (2004), the transition from collisional to post-collisional magmatism can be explained in terms of a series of crust–mantle interaction processes, which commence with lithospheric stacking, followed by slab breakoff and lithospheric delamination. Such breakoff or delamination allows hot asthenospheric material to well up, promoting melting and leading to underplating of mafic rocks (Schott & Schmeling 1998). These underplated magmas may have provided the heat necessary for melting of the existent mafic to intermediate lower crustal rocks to produce medium- to high-K felsic magmas such as the Sonidzuoqi rhyolites.

Most recently, Jian *et al.* (2010) proposed an intraoceanic arc–trench system above a south-dipping subduction zone on the basis of a geochronological and geochemical study of the ophiolitic rocks from the Solonker suture zone. This resulted in a sequence of Permian tectonic–magmatic events during the life cycle of a suprasubduction-zone-type ophiolite, including pre-subduction (*c.* 299–290 Ma), subduction initiation (*c.* 294–280 Ma) and ridge–trench collision (*c.* 281–273 Ma) (Jian *et al.* 2010). Whereas ridge–trench collision terminates formation of this ophiolite, the mechanism for subduction initiation remains unsolved.

With the documentation of a slab breakoff or delamination regime in the north-dipping subduction system during Early Permian time (this study; Zhang *et al.* 2008; Blight *et al.* 2010*a*), it follows that the north-dipping slab breakoff beneath the northern continental block may have coincided with south-dipping intra-oceanic subduction initiation (Fig. 12). Such synchronicity is a natural corollary rather than a surprise. A modern analogue to slab breakoff as the mechanism for flipping of subduction polarity has been documented in the Taiwan mountain belt (Teng *et al.* 2000), where the breaking off of the east-dipping Eurasian slab beneath the Taiwan orogen in the early Pliocene triggered the north-dipping subduction of the Philippine Sea plate beneath north–central Taiwan. By analogy, we suggest that the slab breakoff of the north-dipping Palaeo-Asian oceanic plate beneath the northern continental block during the Early Permian led to the switch in subduction polarity in the Solonker suture zone and initiated the south-dipping subduction as recorded by the Solonker ophiolite.

Implication for Phanerozoic crustal growth

As in the cases of the New England and Lachlan Fold Belts in southeastern Australia (King *et al.* 1997), the Newfoundland Appalachians in Canada (Whalen *et al.* 1996), the Niger–Nigerian province (Kinnaird & Bowden 1987) and the Arabian–Nubian shield (Mushkin *et al.* 2003), the widespread occurrence of felsic igneous rocks with mantle-like isotopic signatures in the Central Asian Orogenic Belt attest to this being a significant site of Phanerozoic crustal growth (e.g. Wickham *et al.* 1996; Heinhorst *et al.* 2000; Wu *et al.* 2002, 2003; Jahn 2004; Chen & Arakawa 2005; Helo *et al.* 2006; Zhang *et al.* 2008, 2010*a*).

Given the juvenile affinity of the felsic rocks in this study, we adopted the equation of DePaolo *et al.* (1991) that was applied to the Phanerozoic granitoids in the Central Asian Orogenic Belt (Wu *et al.* 2003; Jahn 2004), to estimate the proportions of juvenile components in them. Modelling results show that the juvenile component represents about 91–94% (Fig. 11b), higher than the *c.* 65–90% of juvenile crust in the granites from NE China (Wu *et al.* 2003; Jahn 2004).

In contrast to lateral crustal growth through accretion of arc complexes and subduction-zone magmatism during pre-collisional stages (Sengör *et al.* 1993; Windley *et al.* 2007), this study, together with our previous documentation of Early Permian bimodal volcanic rocks from central Inner Mongolia (Zhang *et al.* 2008) and Late Permian to Early Triassic mafic to felsic intrusive rocks from the North Liaoning Block of north China (Zhang *et al.* 2010*a*), reinforces the increasingly recognized importance of post-collisional to post-orogenic vertical accretion in Phanerozoic continental crustal growth (Jahn 2004). Moreover, these case studies exemplify a crustal continuum

growth model that involves progenitor basaltic extraction, resultant magmatic underplating, intermediary differentiation, juvenile lower crustal anatexis and subsequent magma fractionation.

This model takes a distinctive flavour from the differentiation model of Chen & Arakawa (2005) with reference to the Late Carboniferous granitoids from NW China. The latter visualizes that high-silicic magmas could evolve from contemporaneous basaltic magmas by protracted fractional crystallization during post-collisional extension and thus represent production of juvenile continental crust in the Phanerozoic. This indicates that both mechanisms can convert a basic crust into a felsic one and thus result in voluminous Phanerozoic vertical crustal growth in the Central Asian Orogenic Belt.

Conclusions

SHRIMP zircon U–Pb dating constrains an Early Permian extrusive age of *c.* 289–287 Ma for the late Paleozoic volcanic rocks at Sonidzuoqi in western Inner Mongolia, north China. Geochemical and isotopic tracing indicates that the mafic rocks were probably derived from partial melting of dual subduction-related metasomatized asthenospheric and lithospheric mantle, whereas the felsic ones were formed through partial melting of mixed protoliths composed of predominant newly underplated mafic lower crust and minor ancient crustal materials. This high-potassium mafic and felsic calc-alkaline magmatic association serves as a critical link between Carboniferous calc-alkaline plutonism and Early Permian bimodal volcanism and A-type plutonism. Taken together, they constitute an evolved magmatic system developed on a convergent continental margin and reflect the shift in geodynamic setting from an earlier continental arc environment to a later post-collisional extensional regime. This study not only provides an ancient case example with slab breakoff as the mechanism for flipping of subduction polarity, but also documents a typical case of vertical continental crustal growth within a post- collisional extensional regime of slab breakoff.

We wish to extend our thanks to Qian Mao, Yuguang Ma, He Li, Xindi Jin, Chaofeng Li and Xianghui Li for their help in zircon CL imaging, major and trace element analysis, and Sr–Nd–Pb isotope analysis. We are also grateful to K. Goodenough, M. Sun and subject editor M. Cho for their constructive suggestions, which substantially improved the paper. This study was financially supported by the Knowledge Innovation Program of the Chinese Academy of Sciences (Grants KZCX2-YW-Q4-04 and KZCX2-YW-QN115), the Major State Basic Research Program of the People's Republic of China (Grant 2006CB403504) and the National Natural Science Foundation of China (Grant 90914008). This is The Institute for Geoscience Research (TIGeR) Publication 239.

References

Aguillón-Robles, A., Caimus, T., Bellon, H., Maury, R.C., Cotton, J., Bourgois, J. & Michaud, F. 2001. Late Miocene adakite and Nb enriched basalts from Vizcaino Peninsula, Mexico: indicators of East Pacific Rise subduction below southern Baja California. *Geology*, **29**, 531–534.

Allègre, C.J. & Minster, J.F. 1978. Quantitative models of trace element behavior in magmatic processes. *Earth and Planetary Science Letters*, **38**, 1–25.

Altherr, R., Holl, A., Hegner, E., Langer, C. & Kreuzer, H. 2000. High-potassium, calc-alkaline I-type plutonism in the European Variscides: northern Vosges (France) and northern Schwarzwald (Germany). *Lithos*, **59**, 51–73.

Badarch, G., Cunningham, W.D. & Windley, B.F. 2002. A new terrane subdivision for Mongolia: implications for the Phanerozoic crustal growth of Central Asia. *Journal of Asian Earth Sciences*, **21**, 87–104.

Bao, Q.Z., Zhang, C.J. & Wu, Z.L. 2007. SHRIMP U–Pb zircon geochronology and its implications of Carboniferous period quartz diorite in Baiyingaole area, Inner Mongolia. *Journal of Jilin University (Earth Science Edition)*, **37**, 15–23.

Barbarin, B. 1999. A review of the relationships between granitoid types, origins and their geodynamic environments. *Lithos*, **46**, 605–626.

Barry, T.L. & Kent, R.W. 1998. Cenozoic magmatism in Mongolia and the origin of central and east Asian basalts. *In:* Flower, M.F.J., Chung, S.L., Lo, C.H. & Lee, T.Y. (eds) *Mantle Dynamics and Plate Interactions in East Asia*. Geodynamics Series, American Geophysical Union, **27**, 347–364.

Blight, J.H.S., Crowley, Q.G., Petterson, M.G. & Cunningham, D. 2010*a*. Granites of the southern Mongolia Carboniferous arc: new geochronological and geochemical constraints. *Lithos*, **116**, 35–52.

Blight, J.H.S., Petterson, M.G., Crowley, Q.G. & Cunningham, D. 2010*b*. The Oyut Ulaan volcanic group: stratigraphy, magmatic evolution and timing of Carboniferous arc development in SE Mongolia. *Journal of the Geological Society, London*, **167**, 491–509.

Bonin, B. 2004. Do coeval mafic and felsic magmas in post-collisional to within-plate regimes necessarily imply two contrasting, mantle and crustal, sources? A review. *Lithos*, **78**, 1–24.

Bonin, B., Azzouni-Sekkal, A., Bussy, F. & Ferrag, S. 1998. Alkali-calcic and alkaline post-orogenic (PO) granite magmatism: petrologic constraints and geodynamic settings. *Lithos*, **45**, 45–70.

Borg, L.E. & Clynne, M.A. 1998. The petrogenesis of felsic calc-alkaline magmas from the Southernmost Cascades, California: origin by partial melting of basaltic lower crust. *Journal of Petrology*, **39**, 1197–1222.

Chen, B. & Arakawa, Y. 2005. Elemental and Nd–Sr isotopic geochemistry of granitoids from the West Junggar foldbelt (NW China), with implications for Phanerozoic continental growth. *Geochimica et Cosmochimica Acta*, **69**, 1307–1320.

Chen, B., Jahn, B.M., Wilde, S.A & Xu, B. 2000. Two contrasting Paleozoic magmatic belts in northern Inner Mongolia, China: petrogenesis and tectonic implications. *Tectonophysics*, **328**, 157–182.

Chen, B., Jahn, B.M. & Tian, W. 2009. Evolution of the Solonker suture zone: constraints from zircon U–Pb ages, Hf isotopic ratios and whole-rock Nd–Sr isotope compositions of subduction- and collision-related magmas and forearc sediments. *Journal of Asian Earth Science*, **34**, 245–257.

Clemens, J.D. 2003. S-type granitic magmas—petrogenetic issues, models and evidence. *Earth-Science Reviews*, **61**, 1–18.

Clemens, J.D., Darbyshire, D.P.F. & Flinders, J. 2009. Sources of post-orogenic calcalkaline magmas: the Arrochar and Garabal Hill–Glen Fyne complexes, Scotland. *Lithos*, **112**, 524–542.

Cope, T., Ritts, B.D., Darby, B.J., Fildani, A. & Graham, S.A. 2005. Late Paleozoic sedimentation on the northern margin of the North China block: Implications for regional tectonics and climate change. *International Geology Review*, **47**, 270–296.

Coulon, C., Megartsi, M., *et al.* 2002. Post-collisional transition from calc-alkaline to alkaline volcanism during the Neogene in Oranie (Algeria): magmatic expression of a slab breakoff. *Lithos*, **62**, 87–110.

DePaolo, D.J., Linn, A.M. & Schubert, G.. 1991. The continental crustal age distribution: methods of determining mantle separation ages from Sm–Nd isotopic data and application to the southeastern United States. *Journal of Geophysical Research*, **43**, 771–787.

Duggen, S., Hoernle, K., van den Boggaard, P. & Garbe-Schönberg, D. 2005. Post-collisional transition from subduction- to intraplate-type magmatism in the westernmost Mediterranean: evidence for continental-edge delamination of subcontinental lithosphere. *Journal of Petrology*, **46**, 1155–1201.

Eby, G.N. 1992. Chemical subdivision of the A-type granitoids: petrogenetic and tectonic implications. *Geology*, **20**, 641–644.

Ferré, E. & Leake, B.E. 2001. Geodynamic significance of early orogenic high-K crustal and mantle melts: examples of the Corsica Batholith. *Lithos*, **59**, 47–67.

Fraser, K.J., Hawkesworth, C.J., Erland, A.J., Mitchell, R.H. & Scottsmith, B.H. 1985. Sr–Nd–Pb isotopic and minor element geochemistry of lamprophyres and kimberlites. *Earth and Planetary Science Letters*, **76**, 57–70.

Frost, C.D., Bell, J.M., Frost, B.R. & Chamberlain, K.R. 2001*a*. Crustal growth by magmatic underplating: Isotopic evidence from the northern Sherman batholith. *Geology*, **29**, 515–518.

Frost, B.R., Barnes, C.G., Collins, W.J., Arculus, R.J., Ellis, D.J. & Frost, C.D. 2001*b*. A geochemical classification for granitic rocks. *Journal of Petrology*, **42**, 2033–2048.

Goodenough, K.M., Thomas, R.J., *et al.* 2010. Post-collisional magmatism in the central East African Orogen: the Maevarano Suite of north Madagascar. *Lithos*, **116**, 18–34.

Guo, F., Fan, W., Li, C., Gao, X. & Miao, L. 2009. Early Cretaceous highly positive ε_{Nd} felsic volcanic rocks from the Hinggan mountains, NE China: origin and implications for Phanerozoic crustal growth. *International Journal of Earth Science*, **98**, 1395–1411.

Harris, N.B.W., Pearce, J.A. & Tindle, A.G. 1986. Geochemical characteristics of collision zone magatism. *In:* Coward, M.P. & Ries, A.C. (eds) *Collision Tectonics*. Geological Society, London, Special Publications, **19**, 67–82.

Hart, S.R. 1984. A large-scale isotope anomaly in the Southern Hemisphere mantle. *Nature*, **309**, 753–757.

Heinhorst, J., Lehmann, B., Ermolov, P., Serykh, V. & Zhurutin, S. 2000. Paleozoic crustal growth and metallogeny of Central Asia: Evidence from magmatic–hydrothermal ore systems of Central Kazakhstan. *Tectonophysics*, **328**, 69–88.

Helo, C., Hegner, E., Kroner, A., Badarch, G., Tomurtogoo, O., Windley, B.F. & Dulski, P. 2006. Geochemical signature of Palaeozoic accretionary complexes of the Central Asian Orogenic Belt in southern Mongolia, constraints on arc environments and crustal growth. *Chemical Geology*, **227**, 236–257.

Hoffman, A.W. 2003. Sampling mantle heterogeneity through oceanic basalts: isotopes and trace elements. *In:* Carlson, R.W. (ed.) *The Mantle and Core. Treatise in Geochemistry, Vol. 2*. Elsevier–Pergamon, Oxford, 61–102.

Huppert, H. & Sparks, R.S.J. 1988. The generation of granitic magmas by intrusion of basalt into continental crust. *Journal of Petrology*, **29**, 599–624.

IMBGMR 1980. *1:200000 scale geological map of Bayinwula*. Inner Mongolian Bureau of Geology and Mineral Resources, Hohhot.

Jacobs, J., Bingen, B., Thomas, R.J., Bauer, W., Wingate, M.T.D. & Feitio, P. 2008. Early Palaeozoic orogenic collapse and voluminous late-tectonic magmatism in Dronning Maud Land and Mozambique: insights into the partially delaminated orogenic root of the East African–Antarctic Orogen. *In:* Satish-Kumar, M., Motoyoshi, Y., Osanai, Y., Hiroi, Y. & Shiraishi, K. (eds) *Geodynamic Evolution of East Antarctica: A Key to the East–West Gondwana Connection*. Geological Society, London, Special Publications, **308**, 69–90.

Jahn, B.M. 2004. The Central Asian Orogenic Belt and growth of the continental crust in the Phanerozoic. *In:* Malpas, J., Fletcher, C.J.N., Ali, J.R. & Aitchison, J.C. (eds) *Aspects of the Tectonic Evolution of China*. Geological Society, London, Special Publications, **226**, 73–100.

Jian, P., Liu, D.Y., *et al.* 2008. Time scale of an early to mid-Paleozoic orogenic cycle of the long-lived Central Asian Orogenic belt, Inner Mongolia of China: Implications for continental growth. *Lithos*, **101**, 233–259.

Jian, P., Liu, D.Y., *et al.* 2010. Evolution of a Permian intraoceanic arc–trench system in the Solonker suture zone, Central Asian Orogenic belt, China and Mongolia. *Lithos*, **118**, 169–190.

Jiang, G.Q., Zhang, W.J., Xiao, R.G., Luo, Z.H., Li, S.J. & Gao, D.Z. 1995. Subdivision and correlation of Permian strata in Sonidzuoqi area, Inner Mongolia. *Journal of Graduate School, China University of Geosciences*, **9**, 149–161.

Jung, S., Mezger, K. & Hoernes, S. 1998. Petrology and geochemistry of syn- to post-collisional metaluminous A-type granites—a major and trace element and Nd–Sr–Pb–O-isotope study from the Proterozoic Damara Belt, Namibia. *Lithos*, **44**, 147–175.

King, P.L., White, A.J.R., Chappell, B.W. & Allen, C.M. 1997. Characterization and origin of aluminous A-type granites from the Lachlan Fold Belt, Southeastern Australian. *Journal of Petrology*, **38**, 371–391.

Kinnaird, J. & Bowden, P. 1987. African anorogenic alkaline magmatism and mineralization—a discussion with reference to the Niger–Nigerian province. *Geological Journal*, **22**, 297–340.

Kovalenko, V.I., Yarmoluyk, V.V., *et al.* 2006. Geology, geochronology and geodynamics of the Khan Bogd alkali granite pluton in southern Mongolia. *Geotectonics*, **40**, 450–466.

Kürkcüoğlu, B., Furman, T. & Hanan, B. 2008. Geochemistry of post-collisional mafic lavas from the North Anatolian fault zone, Northwestern Turkey. *Lithos*, **101**, 416–434.

Kuscu, G.G. & Geneli, F. 2010. Review of post-collisional volcanism in the Central Anatolian Volcanic Province (Turkey), with special reference to the Tepekoy Volcanic Complex. *International Journal of Earth Science*, **99**, 593–621.

Küster, D. & Harms, U. 1998. Post-collisional potassic granitoids from the southern and northwestern parts of the Late Neoproterozoic East African Orogen: a review. *Lithos*, **45**, 177–195.

Lamb, M.A. & Badarch, G. 2001. Paleozoic sedimentary basins and volcanic arc systems of southern Mongolia; new geochemical and petrographic constraints. *In:* Hendrix, M.S. & Davis, G.A. (eds) *Paleozoic and Mesozoic Tectonic Evolution of Central and Eastern Asia: From Continental Assembly to Intracontinental Deformation*. Geological Society of America, Memoirs, **194**, 117–149.

Landenberger, B. & Collins, W.J. 1996. Derivation of A-type granites from a dehydrated charnockitic lower crust: evidence from the Chaelundi complex, Eastern Australia. *Journal of Petrology*, **37**, 145–170.

Le Maitre, R.W. 1989. *A Classification of Igneous Rocks and a Glossary of Terms: Recommendations of the International Union of Geological Sciences Sub-Commision on the Systematics of Igneous Rocks*. Blackwell, Oxford.

Li, J.Y. 2006. Permian geodynamic setting of Northeast China and adjacent regions: closure of the Paleo-Asian Ocean and subduction of the Paleo-Pacific Plate. *Journal of Asian Earth Sciences*, **26**, 207–224.

Liu, J.F, Chi, X.G., *et al.* 2009. Geochemical characteristics of Carboniferous quartz-diorite in the southern Xiwuqi area, Inner Mongolia and its tectonic significance. *Acta Geologica Sinica*, **83**, 365–376.

Lü, Z.C., Hao, L.B., Duan, G.Z., Li, D.C. & Pan, J. 2002. Lithogeochemical characteristics and tectonic implications of two series of volcanic rocks from early Permian Dashizhai Formation in the southern section of Da Hinggan Mountains. *Geochimica*, **31**, 338–346.

Ludwig, K. 2001. *User manual for Isoplot/EX (2.49)*. Berkeley Geochronology Center Special Publications, **1a**.

Lugmair, G.W. & Marti, K. 1978. Lunar initial $^{143}Nd/^{144}Nd$: differential evolution of the lunar crust and mantle. *Earth and Planetary Science Letters*, **39**, 349–357.

Maheo, G., Guillot, S., Blichert-Toft, J., Rolland, Y. & Pecher, A. 2002. A slab breakoff model for the Neogene thermal evolution of South Karakorum and South Tibet. *Earth and Planetary Science Letters*, **195**, 45–58.

Ménard, G. & Molnar, P. 1988. Collapse of a Hercynian Tibetan plateau into a late Palaeozoic European Basin and Range province. *Nature*, **334**, 235–237.

Miao, L., Zhang, F., Fan, W. & Liu, D. 2007. Phanerozoic evolution of the Inner Mongolia–Daxinganling orogenic belt in North China: constraints from geochronology of ophiolites and associated formations. *In:* Zhai, M.G., Windley, B.F., Kusky, T.M. & Meng, Q.R. (eds) *Mesozoic Sub-Continental Lithospheric Thinning under Eastern Asia*. Geological Society, London, Special Publications, **280**, 223–237.

Miao, L.C., Fan, W.M., Liu, D.Y., Zhang, F.Q., Jian, P. & Guo, F. 2008. Geochronology and geochemistry of the Hegenshan ophiolitic complex: implications for late-stage tectonic evolution of the Inner Mongolia–Daxinganling orogenic belt, China. *Journal of Asian Earth Sciences*, **32**, 348–370.

Moghazi, A.M. 2003. Geochemistry and petrogenesis of a high-K calc-alkaline Dokhan volcanic suite, south Safaga area, Egypt: the role of late Neoproterozoic crustal extension. *Precambrian Research*, **125**, 161–178.

Mushkin, A., Navon, O., Halicz, L., Hartmann, G. & Stein, M. 2003. The petrogenesis of A-type magmas from the Amram Massif, southern Israel. *Journal of Petrology*, **44**, 815–832.

Patiño Douce, A.E. & McCarthy, T.C. 1997. Melting of crustal rocks during continental collision and subduction. *In:* Hacker, B.R. & Liou, J.G. (eds) *When Continents Collide: Geodynamics and Geochemistry of Ultrahigh-pressure Rocks*. Kluwer, Dordrecht, 27–55.

Pearce, J.A. 1996. Sources and settings of granitic rocks. *Episodes*, **19**, 120–125.

Pearce, J.A. & Cann, J.R. 1973. Tectonic setting of basic volcanic rocks determined using trace element analyses. *Earth and Planetary Science Letters*, **19**, 290–300.

Pearce, J.A. & Norry, M.J. 1979. Petrogenetic implications of Ti, Zr, Y and Nb variations in volcanic rocks. *Contributions to Mineralogy and Petrology*, **69**, 33–47.

Pearce, J.A., Harris, N.B.W. & Tindle, A.G. 1984. Trace element discrimination diagrams for the tectonic interpretation of granitic rocks. *Journal of Petrology*, **25**, 956–983.

Peccerillo, A. & Taylor, S.R. 1976. Geochemistry of Eocene calc-alkaline volcanic rocks from the Kastamonu area, northern Turkey. *Contributions to Mineralogy and Petrology*, **58**, 63–81.

Pin, C. & Paquette, J.L. 1997. A mantle-derived bimodal suite in the Hercynian belt: Nd isotope and trace element evidence for a subduction-related rift origin of the late Devonian Brevenne metavolcanics, Massif Central (France). *Contributions to Mineralogy and Petrology*, **129**, 222–238.

Roberts, M.P. & Clemens, J.D. 1993. Origin of high-potassium, calcalkaline, I-type granitoids. *Geology*, **21**, 825–828.

Roberts, M.P., Pin, C., Clemens, J.D. & Paquette, J. 2000. Petrogenesis of mafic to felsic plutonic rock associations: the calc-alkaline Quérigut complex, French Pyrenees. *Journal of Petrology*, **41**, 809–844.

Rudnick, R.L. & Gao, S. 2003. Composition of the continental crust. *In:* Rudnick, R.L. (ed.) *The Crust, Treatise in Geochemistry, Vol. 3*. Elsevier-Pergamon, Oxford, 1–64.

Sajona, F.G., Maury, R.C., Bellon, H., Cotton, J. & Defant, M. 1996. High field strength element enrichment of Pliocene–Pleistocene island arc basalts, Zamboanga Peninsula, western Mindanao (Philippines). *Journal of Petrology*, **37**, 693–726.

Schott, B. & Schmeling, H. 1998. Delamination and detachment of a lithospheric root. *Tectonophysics*, **296**, 225–247.

Sengör, A.M.C., Natal'in, B.A. & Burtman, V.S. 1993. Evolution of the Altaid tectonic collage and Palaeozoic crustal growth in Eurasia. *Nature*, **364**, 299–307.

Shao, J.A., Zhang, L.Q., Mu, B.L. & Han, Q.J. 2007. *The exhumation of the Daxinganling and its geodynamic setting*. Geological Publishing House, Beijing.

Shen, S.Z., Zhang, H., Shang, Q.H. & Li, W.Z. 2006. Permian stratigraphy and correlation of Northeast China: a review. *Journal of Asian Earth Sciences*, **26**, 304–326.

Shervais, J.W. 1982. Ti–V plots and the petrogenesis of modern and ophiolitic lavas. *Earth and Planetary Science Letters*, **59**, 101–118.

Shi, G.H., Miao, L.C., Zhang, F.Q., Jian, P., Fan, W.M. & Liu, D.Y. 2004. The age and its regional tectonic implications of the Xilinhot A-type granites, Inner Mongolia. *Chinese Science Bulletin*, **49**, 384–389.

Sisson, T.W., Ratajesti, K., Hankins, W.B. & Glazner, A.F. 2005. Voluminous granitic magmas from common basaltic sources. *Contributions to Mineralogy and Petrology*, **148**, 635–661.

Steiger, R.H. & Jäger, E. 1977. Subcommission on Geochronology; convention on the use of decay constants in geochronology and cosmochronology. *Earth and Planetary Science Letters*, **36**, 359–362.

Stern, R.J. 2002. Subduction zones. *Reviews of Geophysics*, **40**, 1012, doi:10.1029/2001RG000108.

Sun, S.S. & McDonough, W.F. 1989. Chemical and isotopic systematics of oceanic basalts: implications for mantle composition and processes. *In:* Saunders, A.D. & Norry, M.J. (eds) *Magmatism in the Ocean Basins*. Geological Society, London, Special Publications, **42**, 314–353.

Sylvester, P.J. 1989. Post-collisional alkaline granites. *Journal of Geology*, **97**, 261–280.

Teng, L.S., Lee, C.T., Tsai, Y.B. & Hsiao, L.Y. 2000. Slab breakoff as a mechanism for flipping of subduction polarity in Taiwan. *Geology*, **28**, 155–158.

Topuz, G., Altherr, R., *et al.* 2010. Carboniferous high-potassium I-type granitoid magmatism in the eastern Pontides: The Gümüşhane pluton (NE Turkey). *Lithos*, doi:10.1016/j.lithos.2010.01.003.

Wang, K.L., Chung, S.L., O'Reilly, S.Y., Sun, S.S., Shinjo, R. & Chen, C.H. 2004. Geochemical constraints for the genesis of post-collisional magmatism and geodynamic evolution of the Northern Taiwan Region. *Journal of Petrology*, **45**, 975–1011.

Wang, Q., Wyman, D.A., *et al.* 2007. Petrogenesis of Carboniferous adakites and Nb-enriched arc basalts in the Alataw area, northern Tianshan Range (western China): Implications for Phanerozoic crustal growth in the Central Asia orogenic belt. *Chemical Geology*, **236**, 42–64.

Whalen, J.B., Currie, K.L. & Chappell, B.W. 1987. A-type granites: geochemical characteristics, discrimination and petrogenesis. *Contributions to Mineralogy and Petrology*, **95**, 407–419.

Whalen, J.B., Jenner, G.A., Longstaffe, F.J., Robert, F. & Gariepy, C. 1996. Geochemical and isotopic (O, Nd, Pb and Sr) constraints on A-type granite petrogenesis based on the Topsails igneous suite, Newfoundland Appalachians. *Journal of Petrology*, **37**, 1463–1489.

Whitaker, M.L., Nekvasil, H., Lindsley, D.H. & McCurry, M. 2008. Can crystallization of olivine tholeiite give rise to potassic rhyolites?—an experimental investigation. *Bulletin of Volcanology*, **70**, 417–434.

Wickham, S.M., Alberts, A.D., Zanvilevich, A.N., Litvinovsky, B.A., Bindeman, I.N. & Schuble, E.A. 1996. A stable isotope study of anorogenic magmatism in East Central Asia. *Journal of Petrology*, **37**, 1063–1095.

Williams, I.S. 1998. U–Th–Pb geochronology by ion microprobe. *In:* McKibben, M.A., Shanks, W.C. & Ridley, W.I. (eds) *Applications of Microanalytical Techniques to Understanding Mineralizing Processes*. Reviews in Economic Geology, **7**, 1–35.

Williams, H.M., Turner, T.P., Pearce, J.A., Kelley, S.P. & Harris, N.B.W. 2004. Nature of the source regions for post-collisional, potassic magmatism in southern and northern Tibet from geochemical variations and inverse trace element modelling. *Journal of Petrology*, **45**, 555–607.

Windley, B.F., Alexeiev, D., Xiao, W.J., Kroner, A. & Badarch, G. 2007. Tectonic models for accretion of the Central Asian Orogenic belt. *Journal of the Geological Society, London*, **164**, 31–47.

Wu, F.Y., Sun, D.Y., Li, H.M., Jahn, B.M. & Wilde, S.A. 2002. A-type granites in northeastern China: age and geochemical constraints on their petrogenesis. *Chemical Geology*, **187**, 143–173.

Wu, F.Y., Jahn, B.M., *et al.* 2003. Highly fractionated I-type granites in NE China (II): isotopic geochemistry and implications for crustal growth in the Phanerozoic. *Lithos*, **67**, 191–204.

Wu, F.Y., Wilde, S.A., Zhang, G.L. & Sun, D.Y. 2004. Geochronology and petrogenesis of the post-orogenic Cu–Ni sulfide-bearing mafic–ultramafic complexes in Jilin Province, NE China. *Journal of Asian Earth Sciences*, **23**, 781–797.

Xiao, W., Windley, B.F., Hao, J. & Zhai, M. 2003. Accretion leading to collision and the Permian Solonker suture, Inner Mongolia, China: Termination of the central Asian orogenic belt. *Tectonics*, **22**, 1069, doi:10.1029/2002TC001484.

Xiao, W.J., Windley, B.F., Han, C.M., Yuan, C., Sun, M., Li, J.L. & Sun, S. 2009. End Permian to mid-Triassic termination of the southern Central Asian Orogenic Belt. *International Journal of Earth Sciences*, **98**, 1189–1217, doi:10.1007/s00531-008-0407-z.

Yarmolyuk, V.V., Kovalenko, V.I., Salnikova, E.B., Kovach, V.P., Kozlovsky, A.M., Kotov, A.B. & Lebedev, V.I. 2008. Geochronology of igneous rocks and formation of the late Paleozoic south Mongolian active margin of the Siberian continent. *Stratigraphy and Geological Correlation*, **16**, 162–181.

Zhang, S.H., Zhao, Y., Liu, X.C., Liu, D.Y., Chen, F.K., Xie, L. W & Chen, H. H. 2009*a*. Late Paleozoic to Early Mesozoic mafic–ultramafic complexes from the northern North China Block: Constraints on the composition and evolution of the lithospheric mantle. *Lithos*, **110**, 229–246.

Zhang, S.H., Zhao, Y., *et al.* 2009*b*. Contrasting Late Carboniferous and Late Permian–Middle Triassic intrusive suites from the northern margin of the North China craton: geochronology, petrogenesis and tectonic implications. *Geological Society of America Bulletin*, **121**, 181–200.

Zhang, X.H. & Zhai, M.G. 2010. Magmatism and its metallogenetic effects during the Paleozoic continental crustal construction in northern North China: An overview. *Acta Petrologica Sinica*, **26**, 1329–1341.

Zhang, X.H., Zhang, H.F., Tang, Y.J., Wilde, S.A. & Hu, Z.C. 2008. Geochemistry of Permian bimodal volcanic rocks from Central Inner Mongolia, North China: Implication for tectonic setting and Phanerozoic continental growth in Central Asian Orogenic Belt. *Chemical Geology*, **249**, 261–281.

Zhang, X.H., Wilde, S.A., Zhang, H.F., Tang, Y.J. & Zhai, M.G. 2009. Geochemistry of hornblende gabbros from Sonidzuoqi, Inner Mongolia, North China: implication for magmatism during the final stage of suprasubduction zone ophiolite formation. *International Geology Review*, **51**, 345–373.

Zhang, X.H., Zhang, H.F., Wilde, S.A., Yang, Y.H. & Chen, H.H. 2010*a*. Late Permian to early Triassic mafic to felsic intrusive rocks from North Liaoning, North China: Petrogenesis and implication for Phanerozoic continental growth. *Lithos*, **117**, 283–306.

Zhang, X.H., Zhang, H.F., Jiang, N., Zhai, M.G. & Zhang, Y.B. 2010*b*. Early Devonian alkaline intrusive complex from the northern North China Craton: a petrologic monitor of post-collisional tectonics. *Journal of the Geological Society, London*, **167**, 717–730.

Zhou, M., Lesher, M.L. & Yang, Z. 2004. Geochemistry and petrogenesis of 270 Ma Ni–Cu–(PGE) sulfide-bearing mafic intrusions in the Huangshan district, Eastern Xinjiang, Northwest China: Implications for the tectonic evolution of the Central Asian orogenic belt. *Chemical Geology*, **209**, 233–257.

Zhu, Y.F., Sun, S.H., Gu, L.B., Ogasawara, Y., Jiang, N. & Honwa, H. 2001. Permian volcanism in the Mongolian orogenic zone, northeast China: geochemistry, magma sources and petrogenesis. *Geological Magazine*, **138**, 101–115.

Zindler, A. & Hart, S.R. 1986. Chemical geodynamics. *Annual Review of Earth and Planetary Sciences*, **14**, 493–571.

Received 3 June 2010; revised typescript accepted 2 November 2010.
Scientific editing by Moonsup Cho.